The design of Zr metal-organic frameworks in the detection and neutralization of organophosphorus based nerve agents and pesticides

Devin Scott Moore

A graduate thesis submitted in partial fulfillment

of the requirements for the degree of

Master of Science in Chemistry

ABSTRACT

Organophosphates are ubiquitous in uses ranging from chemical warfare agents (CWA's) to detergents. In between these two extreme uses lie organophosphorus-based agrichemicals, primarily pesticides, which are applied in multi-tonne amounts each year. Metal-organic frameworks, especially the UiO-6x family, are known to interact, sequester, and/or break down organophosphate nerve gases.

This thesis presents the synthesis and characterization of UiO-6x MOFs, comparing standing solvothermal with microwave methods, which appear (by powder X-ray diffraction, X-ray photoelectron spectroscopy, and solid-state nuclear magnetic resonance (SS-NMR) analysis) to give equally high-quality products. Preparation of the UiO-6x MOFs were conducted using 1 molar equivalent of $ZrCl_4$ to 1 equivalent of organic ligand in the presence of equal volumes of dimethyl formamide (DMF) and glacial acetic acid (GAA) for both solvothermal and microwave methods. Yields ranged from 41-63% for our synthesized MOFs (UiO-66, UiO-67 and UiO-67-bipy).

The prepared MOFs are then reacted with organophosphate nerve agent simulants and agrichemicals in reactions followed by GC or HPLC; it appears that the studied agrichemicals are less-reactive than their chemical warfare agent equivalents with only (2-chloroethyl) phosphonic acid and glyphosate showing reactivity with UiO-67 and UiO-66 respectively whereas UiO-67-bipy was shown to nearly completely degrade/sequester dimethyl methylphosphonate. Also presented are preliminary SS-NMR spectra on UiO-66 post-reaction with glyphosate. The line-broadening and restricted rotation that occurs on the combined spectrum suggests the pesticide is incorporated whole into the MOF without degrading.

.

ACKNOWLEDGEMENTS

I would like to thank my thesis supervisor, Dr. Craig MacKinnon, as well as my committee members Dr. Stephen Kinrade and Dr. Michael Campbell, for their guidance and feedback throughout the duration of this project. I would also like to thank Debbie Leach in Chem Stores for consistently supplying our research lab with solvents and other reagents in a timely manner. I would also to acknowledge Brad Miller for his help addressing any technical concerns I had in the lab. A special thank you to Dr. Hou's research group for the use of their CEM 2.0 microwave reactor as well as Dr. Kinrade's SS-NMR rotor and Simultaneous Thermal Analyzer (STA/TGA – DSC).

A special thank you also goes out to Clifford Agyei and Jari Nieminen, my lab-mates in Dr. MacKinnon's lab, for providing helpful advice and friendship throughout the duration of this project.

LIST OF TABLES

Page

LIST OF FIGURES

Page

LIST OF ABREVIATIONS

BE – Binding energy

CEES – 2-chloroethylethylsulfide

CWAs – Chemical warfare agents

DIFP – Diisopropylfluorophosphate

DMF – Dimethylformamide

DMMP – Dimethyl methylphosphonate

DMSO – Dimethylsulfoxide

DSC – Differential Scanning Calorimeter

EFG – Electric field gradients

GAA – Glacial acetic acid

GC - Gas chromatography

HPLC – High-performance liquid chromatography

MAS – Magic-angle spinning

MOFs – Metal-organic frameworks

PXRD – Powder X-ray diffraction

SBU – Secondary building unit

SS-NMR – Solid-state nuclear magnetic resonance

STA - Simultaneous Thermal Analyzer

TEA - Triethyl amine

TGA – Thermogravimetrical analysis

UiO - *Universitetet i Oslo*

XPS – X-ray photoelectron spectroscopy

XRD – X-ray diffraction

TABLE OF CONTENTS

Page

1. INTRODUCTION

1.1. Fundamentals of coordination complexes

Coordination complexes are the result of Lewis acid-base reactions in which certain molecules - typically organic compounds, or ***ligands*** - bond to metal atoms or ions via ***coordinate covalent bonds***. The ligand serves as the Lewis Base supplying both electrons to form the covalent bond.

Coordination complexes are researched extensively since there are a near infinite number of ligand/metal combinations that can yield properties and bonding modes that are different from the starting parent building blocks, and even different from any other known ligand-metal combination. Well documented textbook examples of coordination complexes are known, for example, *cis*-platin ($(NH_3)_2PtCl_2$), a widely prescribed anti-cancer drug [1] (Figure 1).

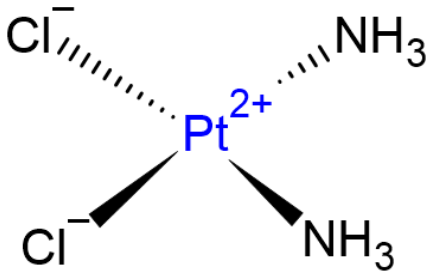

Figure 1 – Structure of *cis*-platin, a Pt^{2+} cation coordinated to 2 NH_3 ligands and 2 Cl^- anions.

Although more recent developments of the metal-ligand relationship tend to focus on complex 2D and 3D supramolecular structures, work with “simple” coordination complexes is ongoing. For example, Wang et al. [2] explored the use of luminescent lanthanide tripyridyl amine, *N,N,N‘,N‘*-tetra(2-pyridyl)-1,4-phenylenediamine and *N,N,N‘,N‘*-tetra(2-pyridyl)biphenyl-4,4‘-diamine coordination complexes as they have

shown promise as emitters in electroluminescent displays. A specific example of one of these complexes is 2,2‘,2‘‘-tripyridylamine (2,2‘,2‘‘-tpa), shown below in Figure 2;

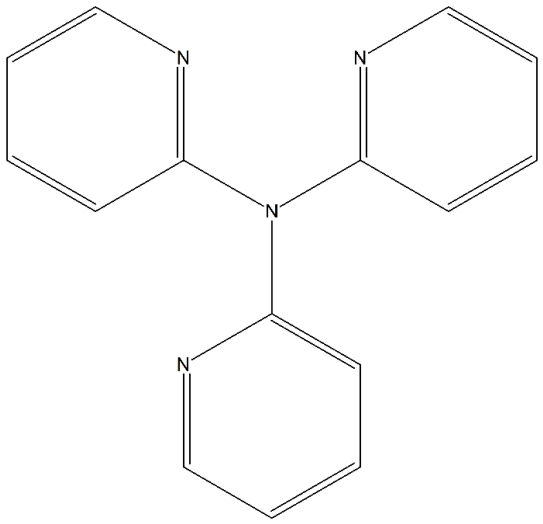

Figure 2 – Structure of 2,2‘,2‘‘-tripyridylamine (2,2‘,2‘‘-tpa) from [2].

1.2. Supramolecular coordination chemistry

More recently, the adaption of coordination compounds to form polymers of alternating organic ligands and metal nodes has been explored. This concept of “node-and-spacer” crystal engineering was first coined by Robson [3] in 1990. It describes the relationship between a metal “node” which controls the shape of the molecule (e.g., octahedral coordination) and bifunctional ligand “spacer” molecules that link the nodes together. Therefore, the larger the organic linker, the larger the space created within the formed cavity of the framework. Beyond simply creating novel compounds, however, functionalization of both the metal nodes and organic spacers has been widely investigated over the course of the last few decades. In the context of solid-state chemistry, coordination polymers and networks have been investigated for their physical properties such as magnetism, color, and luminescence [4]. These properties are attributed to the ability of the combined ligand/metal material to demonstrate properties different from their base components.

For example, Ion et al. constructed 2D coordination networks using anionic polycarboxylate organic spacers and cobalt (II) nodes for the purpose of creating single-ion-magnets (SIMs) [4]. An example of a polycarboxylate organic ligand is shown in Figure 3.

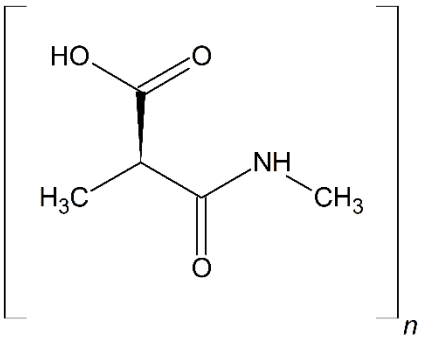

Figure 3 – One isomer of the monomeric building block in polyaspartic acid, an example of a polycarboxylate organic ligand.

1.3. Metal-organic frameworks (MOFs)

Per convention, the terms “coordination polymer” or “coordination solid” are general, and often are used when the coordination networks themselves are functional (e.g., as LEDs or semiconducting materials). The term “metal-organic framework” generally implies that the coordination network is a support scaffold in which interesting properties or chemistry can take place i.e., it is either itself inert to the reaction taking place within, or It is able to be regenerated after the reaction takes place, like a catalyst. Metal-organic-framework’s (MOFs) are a family of crystalline materials composed of metal nodes connected by organic ligands. MOFs have emerged as useful structures for gas storage (H_2, CO_2), gas purification, chemical sensors, and heterogeneous catalysis [5]. Most of these applications are the result of MOFs having a large internal surface area or pore space. The chemical (functional groups) or physical (steric bulk, length) properties, of the MOF can be tailored to the desired use. Two very common

geometric MOF structures are 3D octahedral and 3D hexagonal diamondoid, both of which are shown below in Figure 4.

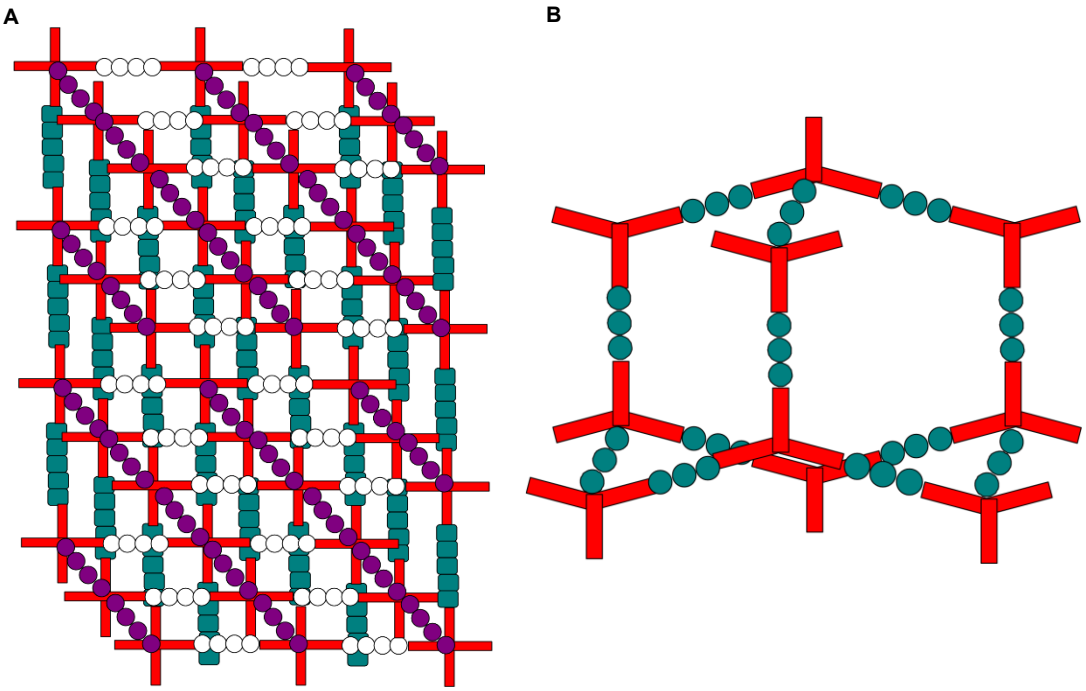

Figure 4 – A) A schematic representation of a 3D octahedral network architecture. Red crosses indicate metal nodes, with white, teal, and magenta circles indicating linkages in different directions. **B)** A schematic representation of a 3D hexagonal diamondoid network architecture. Red indicates metal nodes, with teal circles indicating linkages between nodes. From [6].

1.4. The structure and synthesis of UiO-66 and UiO-67

A potential limitation of single-cation nodes is that they are small and have a limited number of coordination sites. This makes it difficult to create vacant spaces for further exploitation. Such structures tend to form interpenetrating lattices in the solid-state, i.e., the pores are filled with one or more crystallographically independent coordination networks. In other cases, a single network is formed, but it is kept open by incorporating a guest molecule that is integral to the stability of the network, such as a counterion. In the best-case scenario, the pores incorporate a neutral and exchangeable guest such as a solvent molecule. In most of those cases, however, the

limited number of coordination bonds between the nodes and spacers are not strong enough to withstand the loss of the adsorbed guest molecule and the network collapses if it is removed [2].

One way to prevent interpenetrating lattices is to use larger nodes. Larger nodes allow more connections between them to support the empty space. Several metal-oxide clusters have subsequently been identified as large and stable nodes for use in MOFs. One of the most common of these is the $Zr_6O_4(OH)_4^{12+}$ unit. This cluster reacts with organic acids to form three-dimensional structures that can support large open spaces. It accomplishes this by having many inter-node connections (and by its inherent size, preventing interpenetration). Another key advantage is that, in the process of the synthesis the organic acid linkers are deprotonated, and thus act simultaneously as the spacer and the anion (i.e., no space is used up by functionally inert anions).

For this research, the UiO-6x series of MOFs was chosen. The original three are UiO-66, UiO-67, and UiO-68, which all contain the same Zr metal cluster but with different organic linkers, namely terephthalic acid, 4,4'-biphenyldicarboxylic acid, and 4,1':4',4"-terphenyldicarboxylic acid, respectively. In this thesis, only UiO-66 and UiO-67 are used (mainly due to the higher cost of 4,1':4',4"-terphenyldicarboxylic acid).

The UiO-6x series was chosen for this research for their functionality, large internal surface area, robustness, and high thermal stability [7]. UiO-66 was first prepared in 2008 at *Universitetet i Oslo* (University of Oslo, hence the name of UiO) and contains $Zr_6O_4(OH)_4^{12+}$ clusters linked by terephthalate (Figure 5).

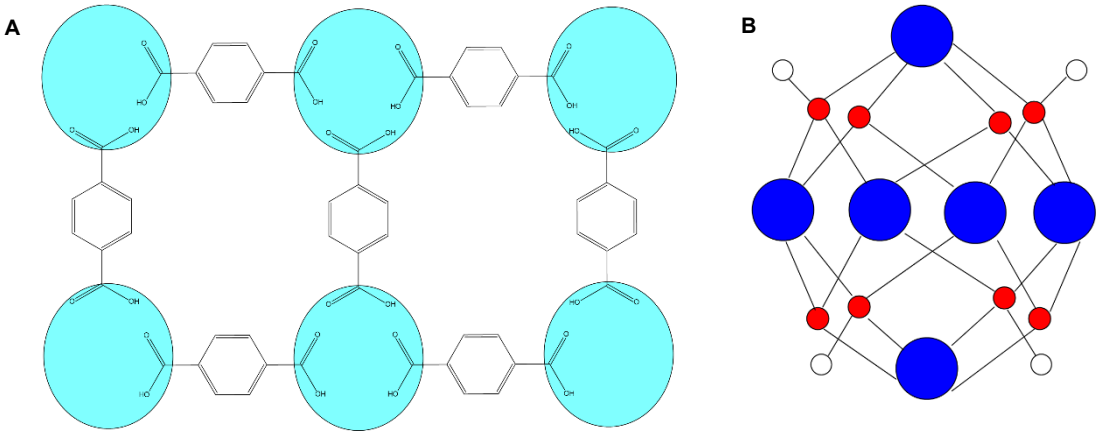

Figure 5 – A) A 2D representation of the **UiO-66 MOF** The teal circles represent $Zr_6O_4(OH)_4^{12+}$ metal clusters linked by terephthalate linker. The exact bonding environment is omitted between the Zr clusters and the ligand for clarity. **B)** A 2D representation of an individual $Zr_6O_4(OH)_4^{12+}$ metal cluster where blue = Zr, red = O, and white = H. On each corner is a Zr^{4+} ion whereas the faces are alternately capped by O^{2-} and OH-. From [7].

As mentioned previously, UiO-67 contains the same Zr cluster but instead linked by 4,4'-biphenyldicarboxylic acid (Figure 6).

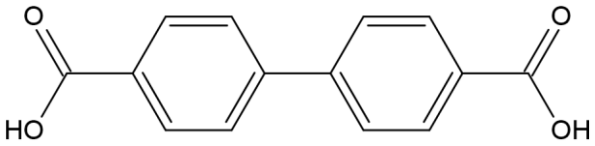

Figure 6 – Structure of 4,4'-biphenyldicarboxylic acid, the linker in UiO-67

If additional substituents exist on the linkers aromatic rings, the naming changes to UiO-6x-Y**,** with Y being the substituent (e.g., $-NH_2$ would indicate an amine R group on the aromatic ring). This convention is also used when the phenyl rings in the diacid are swapped for other aromatic systems such as furan or pyridine (e.g., UiO-67-bipyridine or -bipy when the biphenyl is substituted for bipyridine).

The research presented in this thesis focuses on the UiO-66 and UiO-67 MOFs, including derivatives where the phenyl ring(s) are substituted with other ring systems. Although UiO-6x MOFs exhibit excellent physical properties, their organic linker is functionally inert. One strategy shown by Rodrigo et al. [8] to increase reactivity is to

add substituents to the phenyl rings, such as OH, NH_2, and NO_2. The problem with this is that these functional groups are typically added post-synthetically to the MOF, which can be synthetically difficult, especially in generating homogeneous materials because of the insolubility of these MOFs. Also, the substituents take up valuable space by encroaching on the pores themselves and reducing their size. An alternative is to employ heteroaromatic rings which incorporate nucleophilic and basic sites right in the linker. Two examples are shown in Figure 7, both with a basic nitrogen in the linker ring(s).

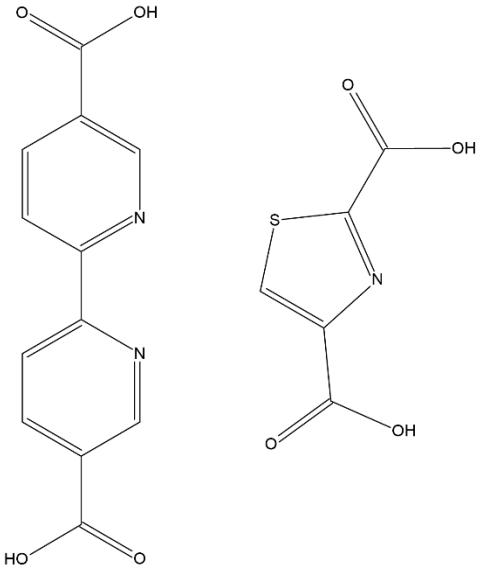

Figure 7 – Heteroatom based organic linkers; 2,2'-Bipyridine-5,5'-dicarboxylic acid(left), 2,4-thiazoledicarboxlyic acid (right).

Regardless of the organic linker molecule used, the MOF synthesis method remains largely common. The most popular methods on the laboratory and industrial scale are solvothermal-based. Solvothermal methods rely on high, consistent temperatures over long periods of time (upwards of 24 h) followed by a slow cool-down period that promotes the crystallization of the MOFs [7]. Currently, one of the most optimized methods employs high-boiling dimethyl formamide (DMF) as the solvent and glacial acetic acid (GAA) as a modulator and holding at least 120°C for 24 hours (e.g., Figure 7).

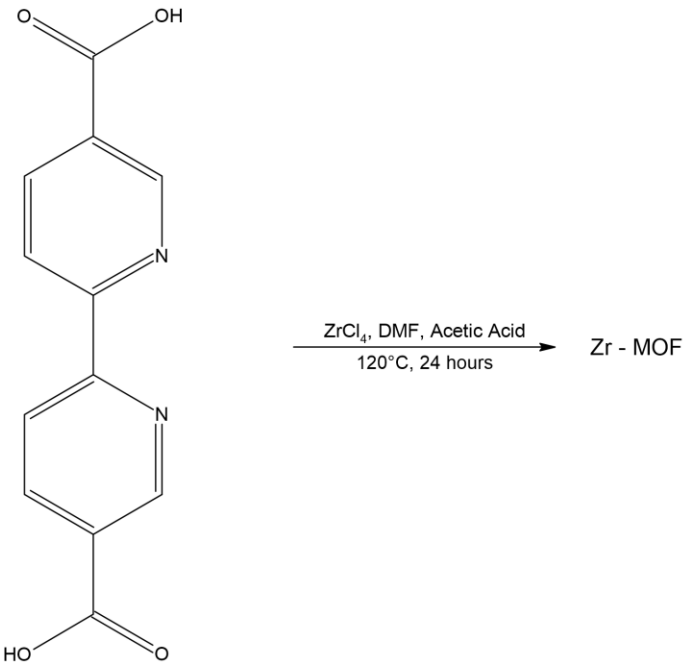

Figure 8 – Proposed solvothermal synthesis method of UiO-67 using 2,2'-bipyridine-5,5'-dicarboxylic acid as the organic linker and $ZrCl_4$ as the source of Zr metal.

The **modulator** is a monocarboxylic acid (RCOOH) that reversibly binds to the metal nodes, slowing the crystal nucleation process and thereby controlling growth of the MOF [7]. Choosing an appropriate amount of a modulator is important, because with too much the crystallization may be entirely inhibited by irreversibly binding to the metal nodes.

Deprotonating agents such as triethylamine (TEA) are sometimes used to "activate" the organic ligands, making it easier to initiate nucleation. A general overview of the mechanisms involved in the crystallization process of UiO-66 has been outlined by Winarta et al. [7] (Figure 8).

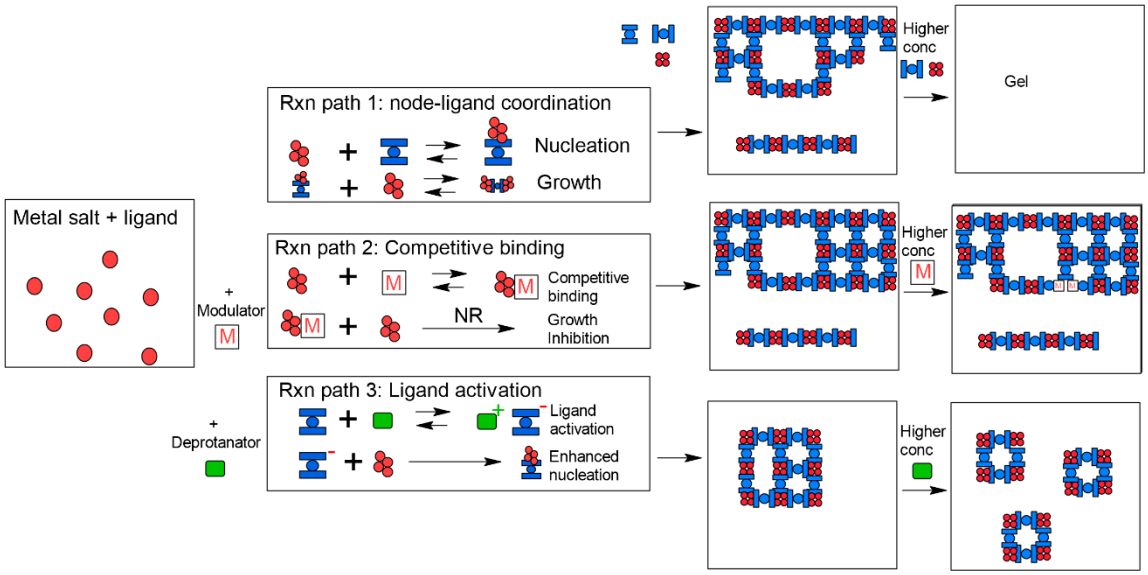

Figure 9 – Summary of potential synthetic outcomes adapted from [7]. Note the growth inhibition and subsequent lack of crystallization as an outcome using a large concentration of modulator, as well as the enhanced nucleation provided when using a deprotonating agent.

1.5. Applications of UiO-66 and UiO-67

Beyond the generic applications of MOFs such as gas storage, separation, and purification, the UiO-6x family is effective for hydrolysis of toxic organophosphates and phosphonates, including nerve agents. These nerve agents, upon entering the body, inhibit the breakdown of acetylcholine by the acetylcholinesterase enzyme. As acetylcholine is responsible for muscular contractions in the body, left unchecked, this will lead to severe muscle spasms and ultimately death [9].

Chemical warfare agents (CWAs) are typically classified under 4 different categories: nerve agents, blistering agents, choking agents and blood agents. Among the more toxic CWAs in these categories are the G (German) and V (Venomous) series nerve agents. G-series nerve agents are extremely volatile liquids at room temperature, making exposure via direct skin contact or inhalation a distinct possibility [9].

Further development of this class of nerve agents led to the even more toxic V-series, which are characterized by their ability to persist on skin, clothes, and other surfaces

due to their low volatility compared to the G-series nerve agents. With their consistency akin to oil, the main risk of exposure is through direct dermal exposure. Several examples of the G and V-series nerve agents are shown below in Figure 10:

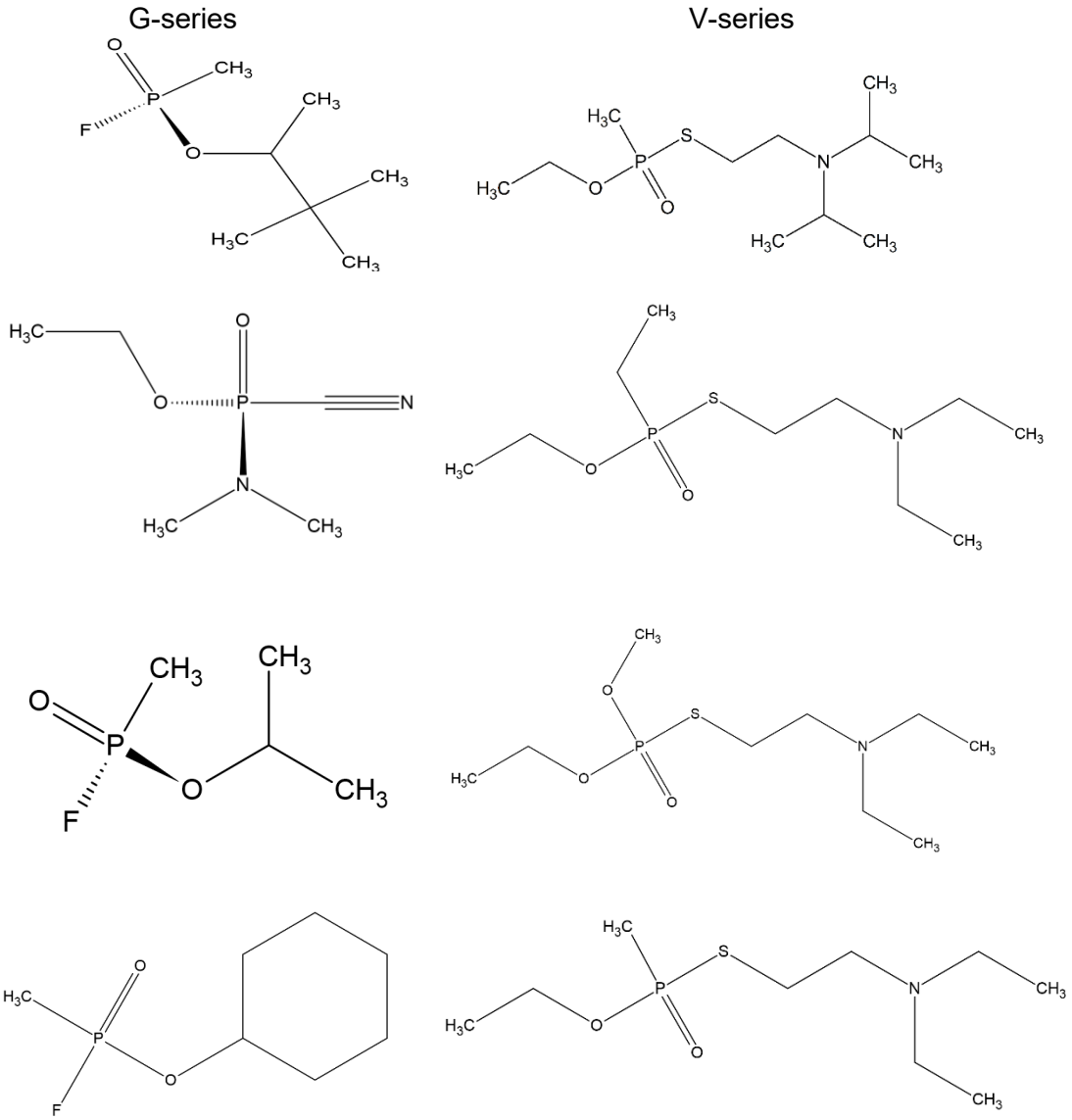

Figure 10 – Structures of the G and V series CWAs. In the (left) G-series column (top to bottom) there is soman (GD), tabun (GA), sarin (GB), and cyclosarin (GF). In the (right) V-series column there is *O*-ethyl-*S*-[2-(diisopropylamino) ethyl] methylphosphonothioate, (VX), *O*-ethyl-*S*-[2-(diethylamino) ethyl] ethylphosphonothioate (VE), *O*,*O*-diethyl-*S*-[2-(diethylamino)ethyl] phosphorothioate (VG), and *O*-ethyl-*S*-[2-(diethylamino)ethyl] methylphosphonothioate (VM)

Although the detoxification of nerve agents is what originally caught the attention of the MacKinnon group with regards to the application of the UiO-6x family of MOFs, the specific exploration of these harmful compounds is a well saturated and well funded field of research [10][11]. However, there are many additional classes of toxic or environmentally disrupting organophosphorus compounds that are commercially used, the most obvious of which are a number of widely applied pesticides.

1.6. Organophosphorus-based pesticides

Many commercially available pesticides have similar structures and properties to the aforementioned CWAs. Two examples are shown in Figures 11 and 12. Some are, in fact, nerve agents that act much more quickly and are more toxic to, for example, ants or aphids than to humans (but chronic exposure is still an issue even for humans). Many of these pesticides are designed to degrade into less toxic phosphate(s), but regardless, combined with phosphates from detergents, there is a general environmental concern regarding their role in the water table [12]. Phosphates promote the exponential growth of algae through the process of **eutrophication**, which often occurs as a result of diffuse agriculture pollution. Although eutrophication is a natural component of the aging process of a body of water, it can be artificially accelerated through human interference. Therefore, the removal of phosphates, or their **sequestration** from the water table is a topic of interest. Phosphorus sequestration refers to the process of removing phosphorus from the water table through physical, chemical, and biological means, and its retention in stable form(s) in the soil [12].

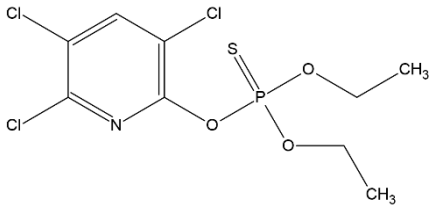

Figure 11 – Structure of chlorpyrifos, an organophosphate insecticide currently undergoing intense regulatory scrutiny in Western Europe and the Americas.

Insecticides and herbicides (e.g., glyphosate, see Figure 12 below) are widely used on a commercial scale, amounting to tonnes of material applied each year in Ontario alone [13]. For example, a 2013-2014 survey from the Ontario Ministry of Agriculture showed that nearly 3 million kilograms (2,909,184kg) of glyphosate was applied to crops. For insecticides, malathion was being used at nearly 5 thousand kilograms (4,858kg) on all surveyed crops [13]. Therefore, exploring the ability of UiO-66 and UiO-67 MOFs to detect, sequester and/or break down these compounds is also of interest. Even though most organophosphate-based pesticides are not that toxic, having these compounds or their by-products persist in the environment is a concern with respect to long term exposure, especially in groundwater as most of these organophosphates are highly soluble in water [12]. One specific consequence of glyphosate being used so frequently is that it has been shown to alter the bacteria inside of bee's guts, making them more susceptible to infection and subsequently death. As nearly 80% of our food is pollinated by bee's, this is extremely concerning [14].

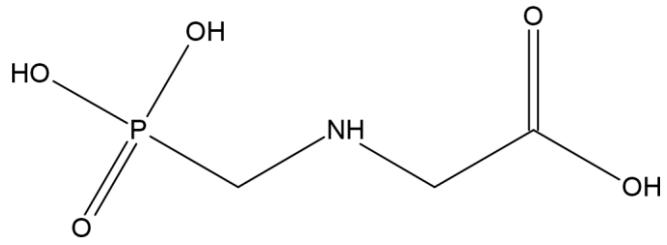

Figure 12 – Structure of glyphosate, an organophosphate herbicide whose potential was realized by Monsanto chemist John E. Franz in 1970. Glyphosate was brought to market under the trade name Roundup.

1.7. Proposed mechanism of degradation

In the previous sections, the need was illustrated for novel compounds and materials that can detoxify these harmful organophosphate-based nerve agents and pesticides. Rodrigo et al. [8] have shown that MOF-like materials should contain nucleophilic and Lewis base sites on the organic linker molecule to promote the hydrolytic degradation of

key P-F and P-Cl bonds within organophosphate-based compounds [15]. An example of this proposed mechanism is shown in Figure 13 using diisopropylfluorophosphate (DIFP):

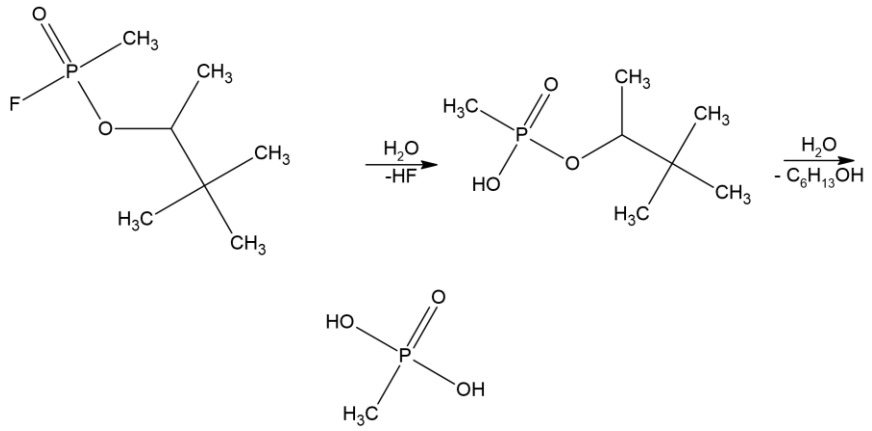

Figure 13 – Hydrolytic degradation of diisopropylfluorophosphate (DIFP) a simulant compound for soman (GD).

The first step is the loss of the key P-F (losing -HF) bond in DIFP through the addition of water. Further addition of water molecules results in the cleavage of the phosphorous moiety of DIFP from the rest of the hydrocarbon chain, leaving three hydrolysis products that are less toxic than the original DIFP.

In a laboratory setting, CWA simulants are often used in place of their more toxic counterparts for obvious reasons. Nerve agents are highly unstable, which is why their mechanism of action is so quick. CWA simulants on the other hand are considerably more resistant to hydrolysis. A consequence of this difference is that if CWA simulants in a laboratory setting are degrading at a reasonable rate, it can be extrapolated that their related nerve agent will break down even quicker. Fortunately, the active ingredients of most organophosphorus pesticides are toxic but can be used in a standard laboratory setting with care. This includes the use of appropriate personal protective equipment (PPE), performing any reactions under a fume hood that contain simulants, as well as appropriate waste disposal.

1.8. Characterization of MOFs in the solid state

The characterization of solid-state materials can be challenging, and MOFs are no different. With most MOFs being insoluble in common organic and inorganic solvents (including their deuterated counterparts), characterizing them in the solid state is realistically the only option. Several analytical techniques can be used to complete the overall characterization of a MOF.

Thermogravimetrical analysis (TGA) can be used to observe key mass changes and determine if our organic linker molecules were being successfully coordinated to our Zr metal centres. Experimental and literature X-ray photoelectron spectroscopy (XPS) spectra can be used to characterize key C-O and Zr-O bonds being formed throughout the course of a reaction (Details of these analyses are given in Chapter 2).

To ascertain the crystallinity of our synthesized MOFs, X-ray diffraction (XRD) data was also used. Similar to XPS, by comparing our experimental spectra with literature results we can determine that we were correctly synthesizing our MOFs. However, this is not a particularly good analytical technique for characterizing new MOFs, like those proposed herein.

Solid state nuclear magnetic resonance (SS-NMR) can provide key structural information based on chemical shifts that other techniques simply cannot. Despite the power of SS-NMR to chemically characterize solids, the technique is not widely used in the MOF literature. Although only a few preliminary spectra were obtained for this project, it is anticipated that SS-NMR will be used extensively as this project goes forward in the future.

1.9. Research proposal

The general goal of this research is to explore the use of the UiO-66 and UiO-67 families of MOFs for the purpose of degrading harmful organophosphate-based CWAs, their simulants, and related pesticides. There are several potential practical uses to this investigation: the development of protective equipment for farmers applying pesticides that incorporates the UiO-6x family of MOFs; the sequestration of phosphate degradation products which prevents them from leaching into groundwater; the use of UiO-6x as a chemical sensor (e.g., determining phosphate levels in a field); and the adsorption (without decomposition) of targeted phosphates, which could extend the potential residency time for certain pesticides (based on the previous work on organophosphate CWAs, it is likely that with small organophosphate pesticides the most likely outcome is decomposition while using the UiO-6x family of MOFs). These are only some of the potential practical outcomes for this research.

Two primary synthesis methods will be compared in this research: solvothermal and microwave assisted. The former of the two is relatively well known in the literature, with the latter being a promising emerging technique to **significantly** cut down on reaction times.

The synthesized MOFs will be characterized via a variety of analytical techniques, with a predominant focus on the use of SS-NMR to gain new insight on the structure of MOFs both before and after reactions. This will help us better understand the mechanism of decomposition. The ability of our synthesized MOFs to degrade several organophosphorus pesticides and CWA simulants will be analyzed in an aqueous environment via gas chromatography (GC) and high-performance liquid chromatography (HPLC). Although preliminary degradation testing was done with CWA

simulants in aqueous environments, a larger focus was placed on organophosphorus-based pesticides (more specifically, their pure, active ingredients).

2. Material Synthesis

2.1. Solvothermal MOF synthesis

Roridgo et al. have shown the ease and practicality of solvothermal synthesis when it comes to creating MOFs [8]. Based on their methods, we were able to develop a general solvothermal synthesis template for creating UiO-66, UiO-67 and UiO-67-bipy MOFs as shown in Figure 15:

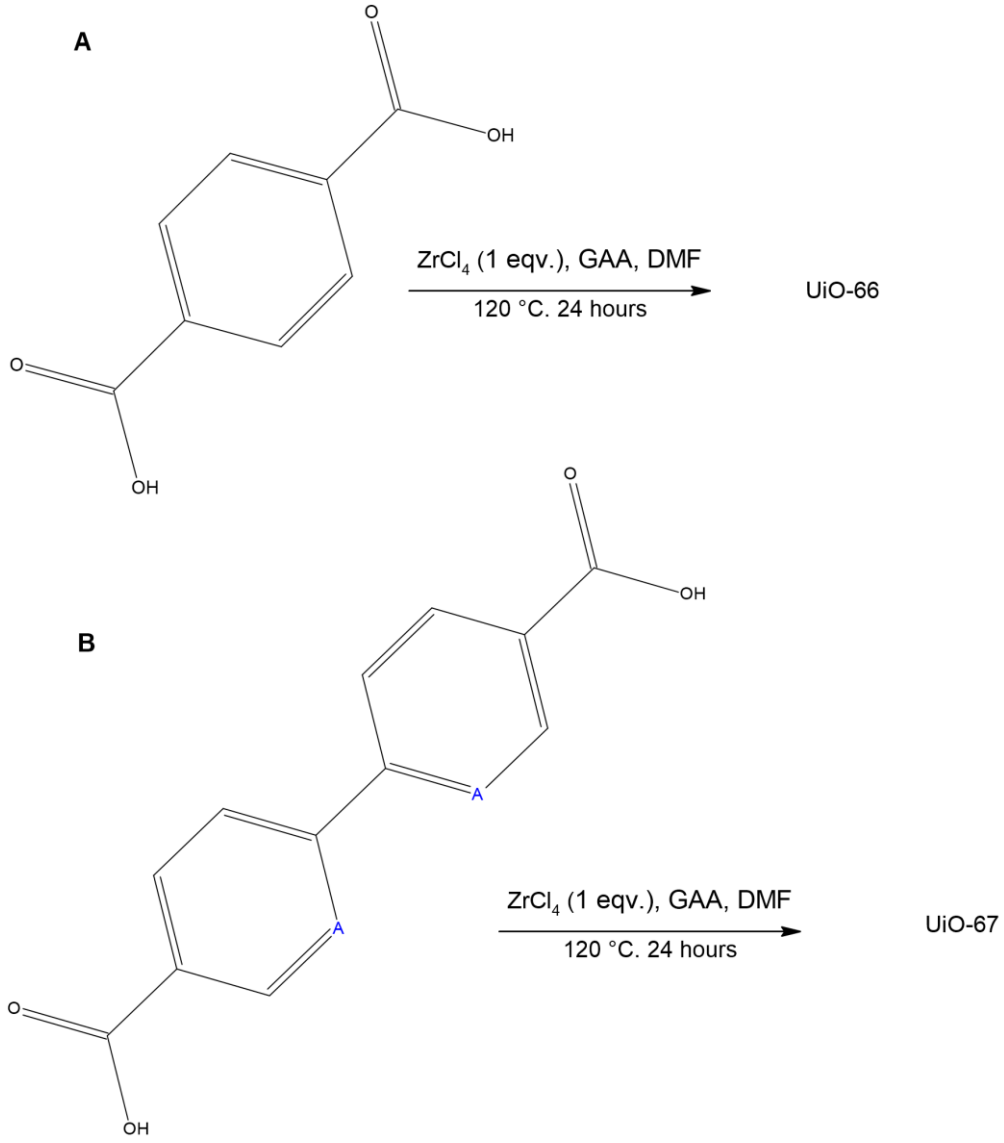

Figure 14 – Generic reaction scheme for the solvothermal synthesis of UiO-66 **A)** and UiO-67 **B)** MOFs. For **B)**, A = CH or N for UiO-67 and UiO-67-bipy respectively. $ZrCl_4$ was used in 1 molar equivalence with the organic ligand. Optimized conditions included 10 mL of GAA and 10 mL of DMF as co-solvents. Yield ranges from 41-63% (see Experimental).

Although it has been shown that the amount of acetic acid modulator can have an affect on pore size in the MOF [7], its amount throughout this research was maintained at 10mL for all reactions. Rodrigo et al. [8] demonstrated the successful synthesis of the base forms of UiO-66 (X = terephthalic acid) and UiO-67 (X = 4,4'-biphenyldicarboxylic acid) by this method. Their reaction conditions were replicated here. The workup of these materials following this reaction period is equally important. Following the heating period, the suspension is brought to room temperature at which point the microcrystalline powder is collected via glass filter frit. The powder is then washed with excess DMF to remove any potentially trapped solvent and then dried with acetone to remove any potential water. To further ensure dryness, the powder is placed in a vacuum desiccator overnight in the presence of P_2O_5 to remove any remaining moisture. This two-step process highlights the robustness of this particular MOF – it survives both the high temperature but also the loss of its guest without changing its structure or degrading (the results of such testing are shown later in this chapter as well as in Chapter 3).

As mentioned previously, the incorporation of nucleophilic (and basic sites) was shown to increase the hydrolytic degradation of CWA simulants in aqueous environments [8][15]. Rodriogo et al. showed that functionalizing their organic linkers with amino (-NH_2) groups increased reactivity compared to that of standard UiO-66. As can be seen from the structure in Figure 15, this amino group sticks out into the space between the nodes, i.e., into the pores of the MOF. Also shown in the Figure are lithium cations

because of the synthetic route used to aminate (lithiation of benzene using LiO^tBu was the first synthetic step).

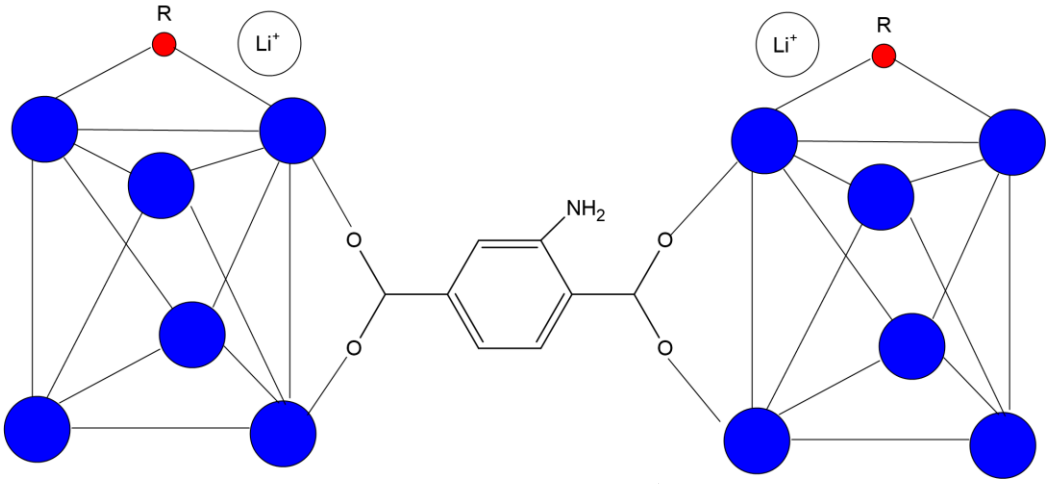

Figure 15 – Generic structure of UiO-66-$x$$NH_2$@Li$O^tBu$ from Rodrigo et al. Blue = Zr metal ions and red = oxygen atoms. Note the amine group on the single phenyl ring as well as the Li^+ ion present in the oxohydroxometallic Zr metal cluster(s).

As mentioned in Figure 15, **2,2'-bipyridine-5,5'-dicarboxylic acid** was also investigated as a ligand. Although this ligand has seen exposure in some MOF research such as gas storage/separation [16], it has not been as widely studied in the CWA degradation literature in spite of the obvious feature of incorporating the nucleophilic site right into the ring system which conserves the pore size of the MOF, as well as eliminating all post-synthetic modifications using amino/Li groups while keeping the functionality of those groups.

These three solvothermally generated MOFs (UiO-66. -67, and -67-bipy) were used to validate the various characterization methods, as detailed in the following 4 sections.

2.2. TGA analysis of UiO-67-bipy

Preliminary characterization of this MOF was done via **thermogravimetrical analysis (TGA)** in an attempt to see if we were generating ZrO_2 (which is the presumed residue based on previous work [17]) *in situ*, being the end product of the decomposition of the **$ZrO_4(OH)_4^{(12+)}$** secondary building unit **(SBU)**. This would also determine whether the

2,2'-bipyridine-5,5'-dicarboxylic acid ligand was donating the required oxygen atoms to form the UiO-67-bipy SBU. The rough coordination environment between the Zr metal clusters and the bipy ligand are shown in Figures 4(a) and 15.

TGA analysis of dry UiO-67-bipy was done with a **Simultaneous Thermal Analyzer (STA, see Experimental)**, with the key details from this analysis highlighted in the red boxes in Figure 16:

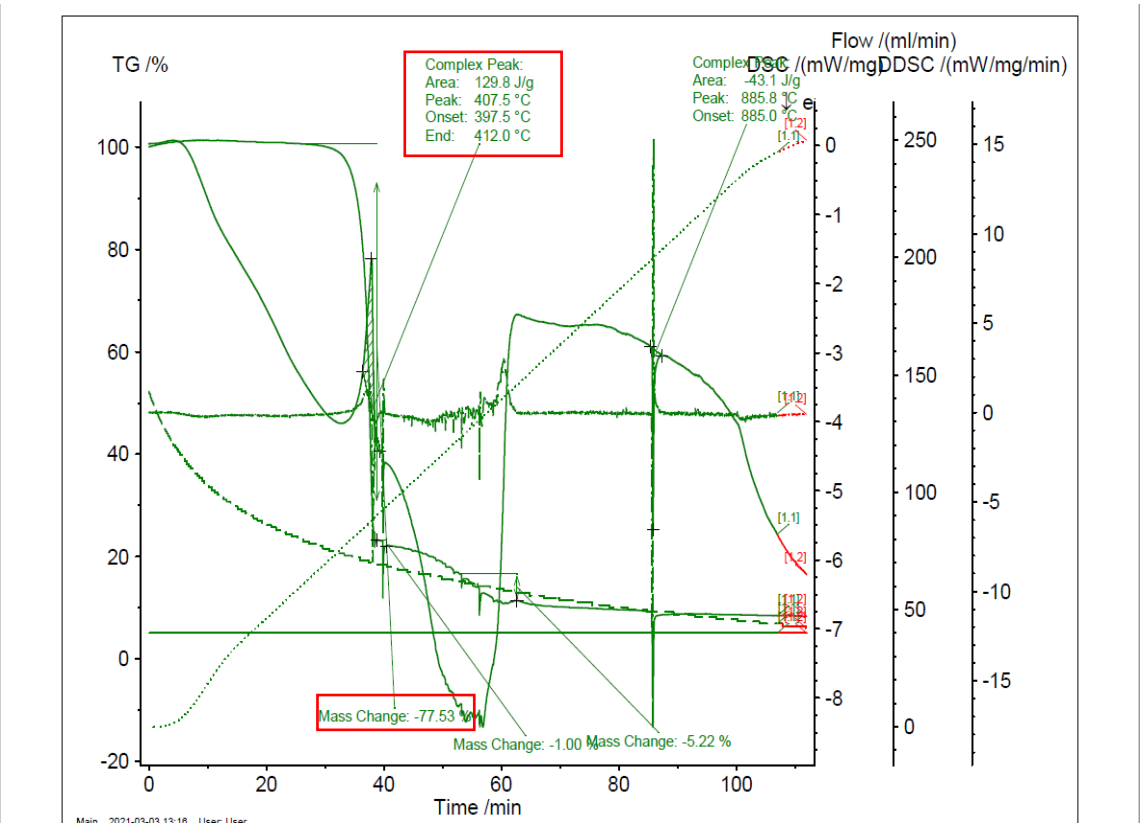

Figure 16 – TGA and DSC analysis of UiO-67-bipy. Note that at 412 °C a 77.53% mass drop is reported.

Figure 16 shows the TGA analysis of UiO-67-bipy run under inert atmosphere conditions. The 77.53% mass loss correlates to our 2,2'-bipyridine-5,5'-dicarboxylic acid ligand missing 2 O atoms ($C_{12}H_6N_2O_2$). This is interpreted as the ligand donating **two O** atoms, **forming ZrO_2**. Little else can be derived from Figure 16 alone, but it does reflect the result we were expecting to see given the reaction conditions we used [18].

2.3. XPS

2.3.1. XPS overview

X-ray photoelectron spectroscopy (XPS) was used as a further characterization method to determine the exact nature of the bonds being formed in our material. XPS is a surface-sensitive spectroscopic technique based on the photoelectric effect (the emission of electrons when EM radiation hits a material). One can determine surface elemental composition chemical states and the general electronic environment of a material.

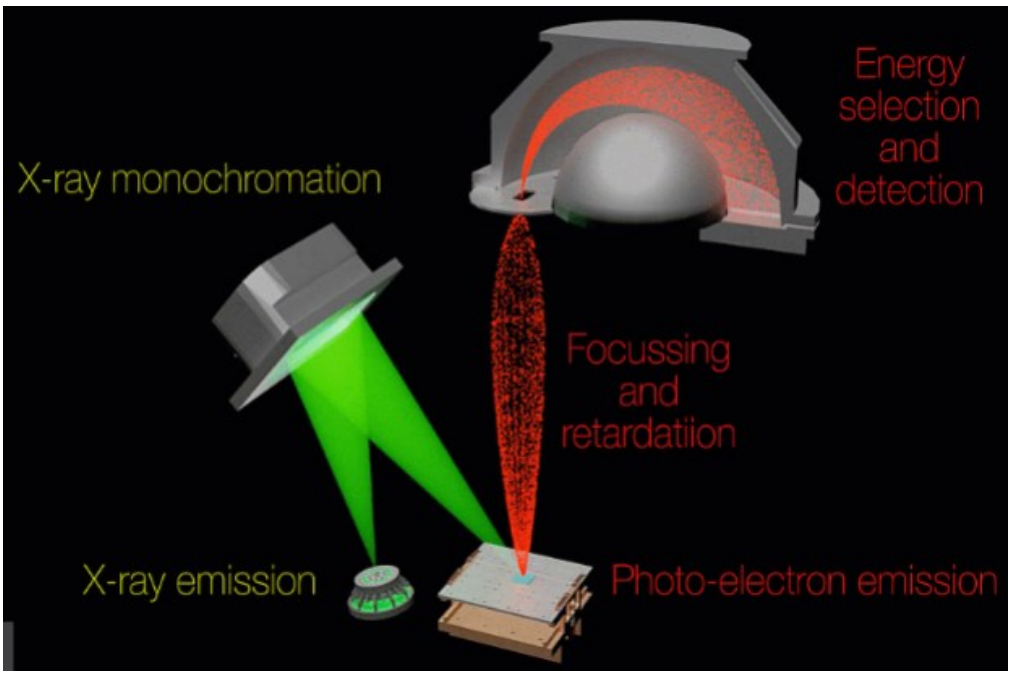

Figure 17 – Diagram explaining the process of monochromatic (i.e., single wavelength) XPS [19].

When an atom/molecule absorbs an X-ray photon, there is a chance an electron will be ejected from an orbital. The kinetic energy (KE) of this electron depends on a couple of factors. Namely, the photon energy (hv) (which depends on the instrument x-ray source), and the binding energy (BE) of the electron (the E required to remove the electron from the surface). BE is affected by a variety of things as well, including: the

element from which the electron is emitted, what orbital the electron is in (closer to core nucleus will have a higher BE) and the chemical environment of the atom from which the electron is emitted. X-rays are energetic enough that core electrons, often as low as the 1s orbital, are emitted rather than valence electrons.

An XPS spectrum is typically a plot of electrons counted at a specific binding energy (in eV). Elements will produce characteristic and unique line spectra based on the respective energy levels of each filled atomic orbital. Each element will produce characteristic XPS peaks based on the electron configuration of that atom (1s, 2s, 2p etc…) at the surface level. Further, local bonding will slightly alter the orbital energies (e.g., electronegativity of bonded neighbours), so an analysis of energy shifts will help elucidate the bonding environment of each element.

A wide-range XPS “survey scan” shows all the elements present *i.e.,* the elemental analysis of the surface. Subsequent high-resolution scans of specific binding energy ranges for individual atoms are run to analyze chemical shifts gives insight to the chemical environment of each element. An example of both types of scans is shown in Figure 19. Note that even at high resolution, the changes in energy for different environments is small compared to the line widths of the peaks, so a deconvolution routine must be applied to deconvolute the number of different bonding environments.

Deconvolution refers to the identification of the “peaks within the peaks” which is necessary when more than one chemical environment exists at the surface for a given atom. This deconvolution is a mathematical model that uses overlapping Gaussian peaks to recreate the observed spectrum. The middle (energy at the maximum peak height) of each of these Gaussian peaks corresponds to the energy of each chemical

environment of the orbital giving rise to the observed XPS peak. Figure 18 shows a survey scan as well as deconvoluted high-resolution spectra:

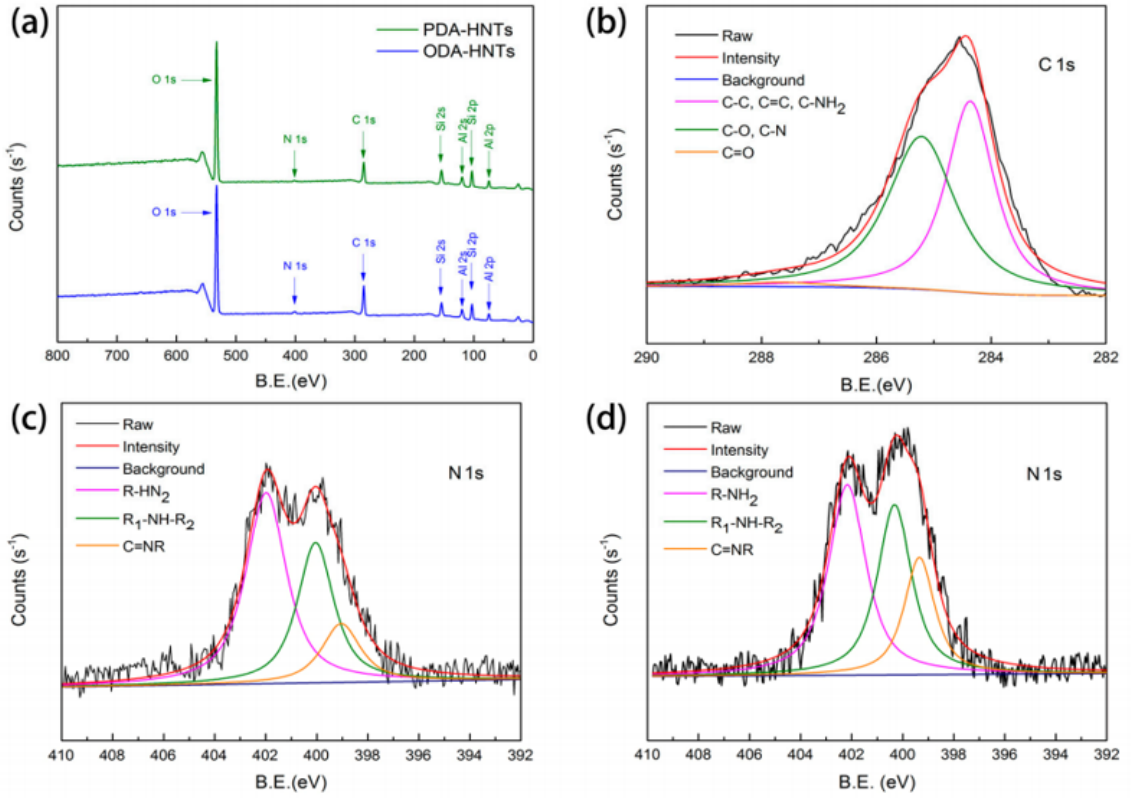

Figure 18 – Example of a survey scan of a typical organic compound (a) with subsequent high-resolution scan (noting the deconvolution) of the C 1s (b) and N 1s (c, d) regions [20].

Table 1: Approximate binding energy ranges for relevant atoms

Atom	Approximate binding energy (eV) [19]
C 1s	284
O 1s	529-530
Zr 3d	179-182
N 1s	298-400

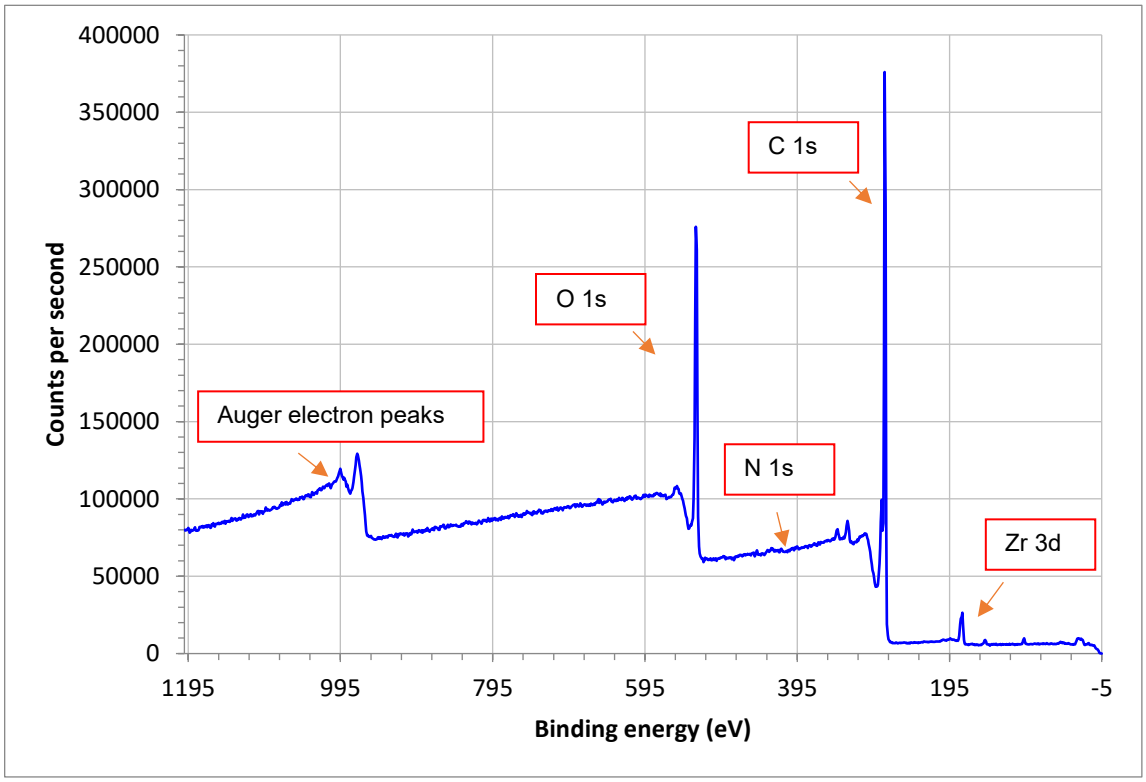

Figure 19 – Example survey scan of our UiO-67-bipy synthesized using solvothermal methods.

The **auger electron/effect** is the result of an inner shell vacancy in an atom being filled by an outer shell electron, resulting in the emission of a photon from the same atom. These auger peaks are automatically generated in the XPS experiment, but they are not particularly useful in determining structural information in this case.

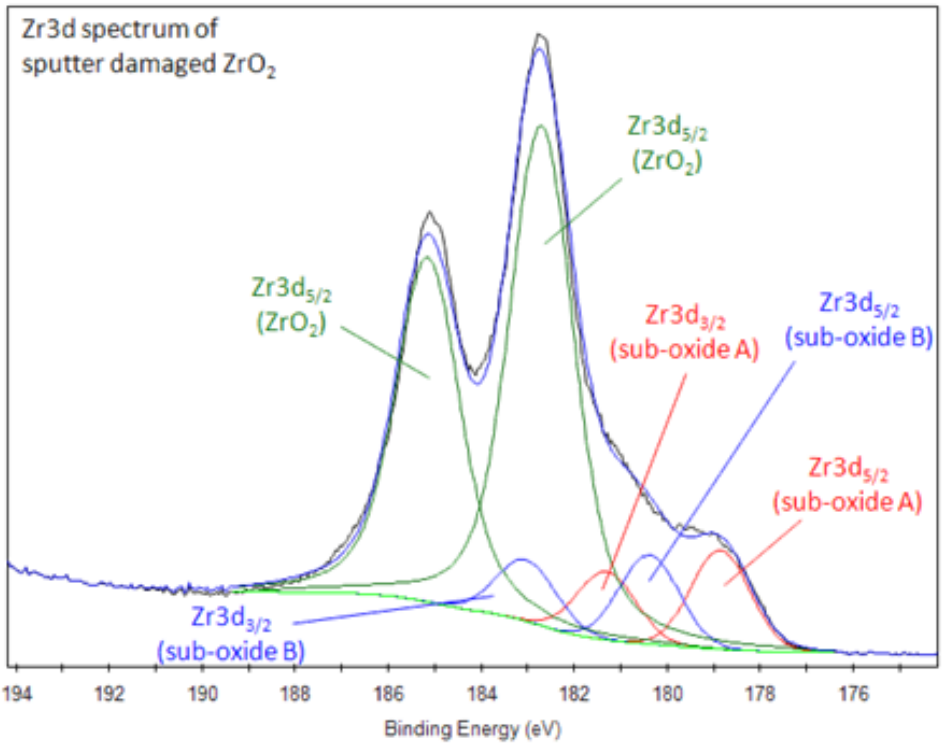

Figure 20 – High-resolution literature [19] scan of the Zr 3d region of Zr(IV)O_2.

Also note that the Zr 3d region is split into two separate peaks is a result of **spin-orbit splitting** or **j-j coupling**. Based on the formula $j = l + s$ (where l = angular momentum quantum number, s = spin angular momentum quantum number, which can be +/- 1/2), all subshells except for the s (where $l = 0$) level gives rise to two possible states with unique binding energies.

We chose to examine the Zr 3d (Figure 20) and O 1s regions of our materials. Li et. al [12] examined the O 1s region of UiO-66. Their findings were used as a point of comparison for our UiO-66, -67, and -67-bipy. The UiO-67-bipy does not appear to have been studied by XPS prior to our investigation.

2.3.2 XPS characterization of UiO-66, UiO-67, and UiO-67-bipy

Figure 21 illustrates a well-resolved spectrum for our generated UiO-66 MOF. For comparison, the literature spectrum of UiO-66 [21] and analysis is shown in Figure 22. The O region is deconvoluted assuming three underlying peaks, i.e., from left to right (higher to lower energy) COOH, Zr-O-C, and Zr-O-Zr. It is clear from the line shape that the Zr-O-C is the largest portion of the peak, with the left 'shoulder' being dangling (unreacted) carboxylic acid from the ligand, while the right shoulder is the Zr-O-Zr oxygen within the Zr cluster.

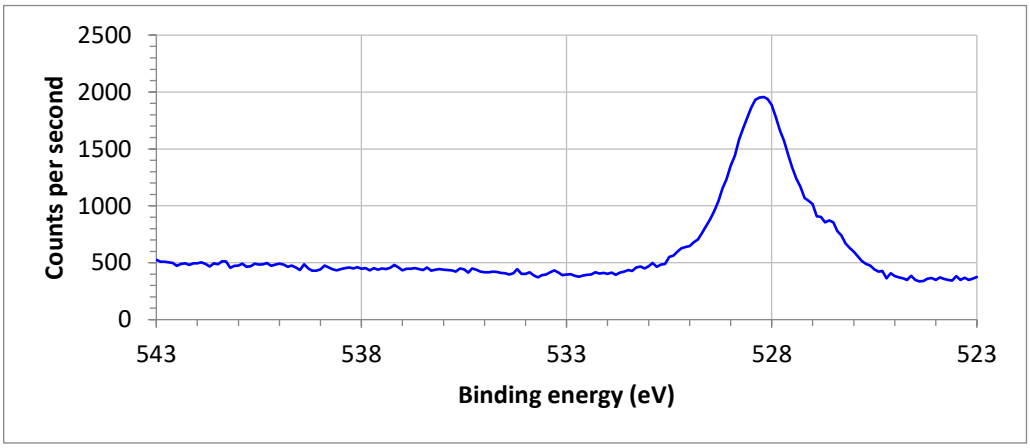

Figure 21 – High-resolution XPS scan of the O 1s region of our synthesized UiO-66 (terephthalic acid ligand).

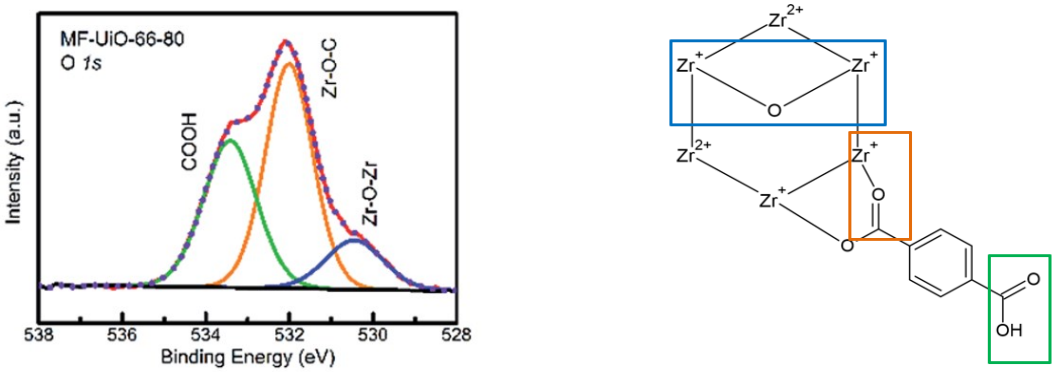

Figure 22 – High-resolution XPS spectra of the O 1s region of UiO-66 (left) from [21] with its deconvoluted structure (based on UiO-66) shown for comparison (right).

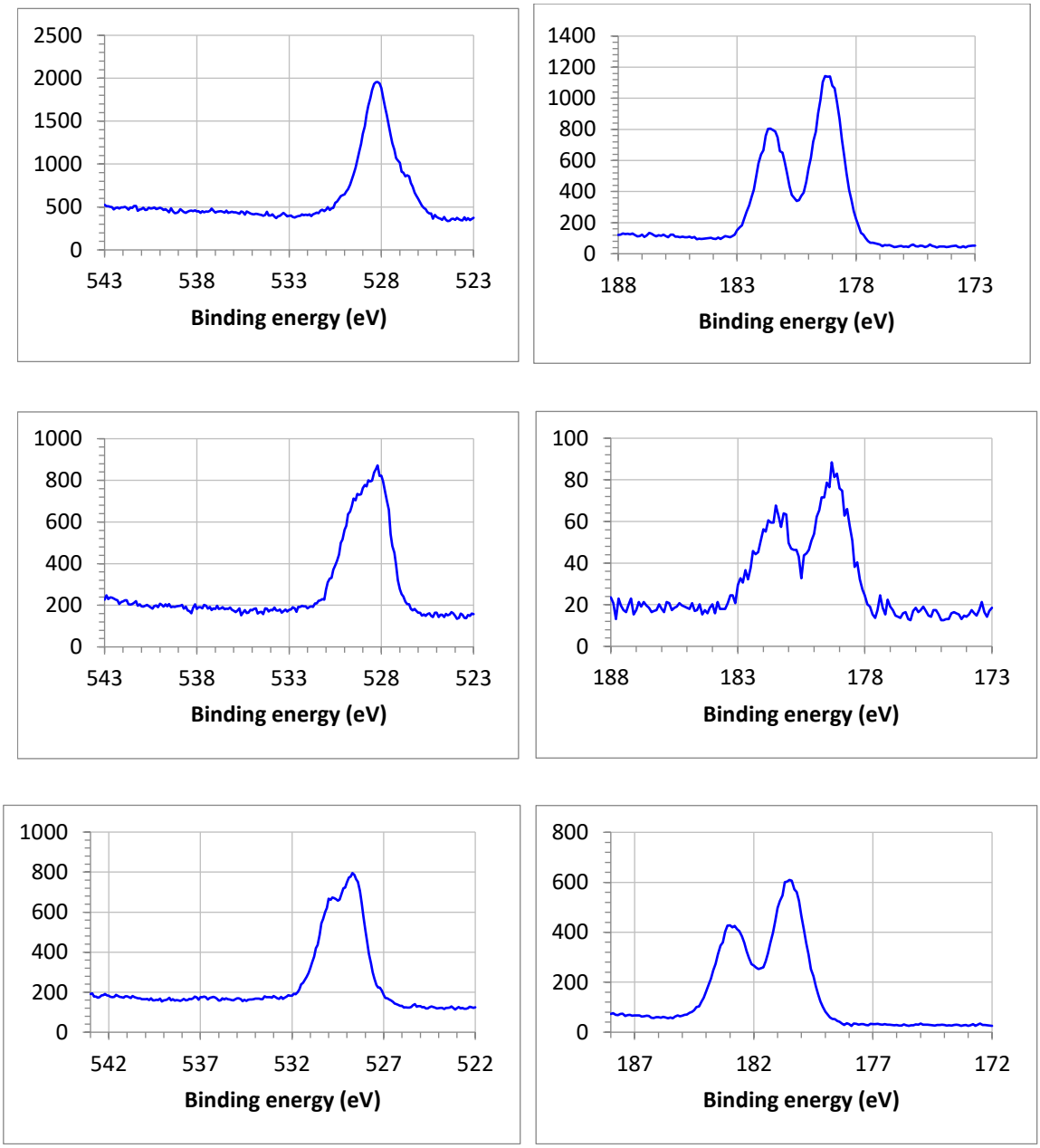

Figure 23 - High-resolution XPS scans of the **O 1s (left column)** and **Zr 3d (right column)** regions of our synthesized **UiO-66 (top row)**, **UiO-67 (middle row)**, and **UiO-67-bipy (bottom row).** The y-axis label is counts per second but is omitted for clarity in this Figure.

The top left spectrum in Figure 23 is the XPS of our UiO-66, zoomed in on the O 1*s* region. The peak shape is almost Gaussian with a very small shoulder on the right, consistent with a deconvolution into the two peaks of the Zr-O-C and Zr-O-Zr bonding environments. There is no evidence to suggest any significant amount of unbound residual COOH present in the sample.

The Zr 3*d* region for the same UiO-66 sample is the top right spectrum of Figure 23. It consists of two well-resolved and well-shaped peaks, which we assign to the split Zr peak corresponding to O-Zr-O bonding environment in the Zr cluster.

The middle row of Figure 23 are the equivalent O 1s and Zr 3d spectra for our synthesized UiO-67. Although the spectra are not as strong (have a higher signal-to-noise ratio), they give the same conclusion. The O 1s spectrum (middle left spectrum) does have a less well-shaped peak, perhaps suggesting a slight unbound free acid character.

Finally, the XPS spectra for our third MOF, UiO-67-bipy, are shown in the bottom row of Figure 23. The O 1s region (bottom left) line shape shows a high frequency (530 eV) shoulder, pointing to some residual COOH character.

When comparing the O 1s literature values for UiO-66 with our experimentally determined values for UiO-67-bipy, Li et al. observed peaks at **530.5, 531.9, 533.3 eV** compared to our experimentally derived values of **527.5, 528.5 and 530 eV**. Although the ligands in the two cases are not the same, the expected local coordination environment of the oxygen should be similar. The overall shape of the peaks is good in comparison, but there is a roughly 2 eV shift when comparing UiO-66 and UiO-67-bipy. We believe that the shift is not “chemical” in nature (difference in bonding environment) but rather was the result of “charge compensation” that is done on non-conductive XPS

samples (as per instrument technician Dr. Guosheng Wu, see Experimental section). The binding energies for non-conductive samples are generally shifted slightly as a result.

Based on these findings, we had further proof that we were generating O-Zr-O in the process of synthesizing our UiO-6x MOFs. Figure 22's deconvoluted spectrum is referenced in comparison with our O 1s spectra in Figure 23 to establish which type of O bonds are most prevalent in our material. In Figure 22, the peak at ~533.3eV represents the COOH character for the O 1s region. Free COOH means uncoordinated carboxylate ligands, which for our materials, is unfavorable. Therefore, the less of this bonding environment we observe, the better. The most COOH character we observed was in our UiO-67-bipy and UiO-67, with UiO-66 showing very little COOH relative to the Zr-O-C and Zr-O-Zr regions. In summary, the XPS spectra suggest very little uncoordinated COOH remains post-synthesis for our MOFs.

2.4. XRD examination of UiO-66 and UiO-67

XRD is a non-destructive technique for analyzing the structure of materials on the atomic and/or molecular level. It is particularly useful for polycrystalline materials. XRD functions by directing a beam of X-rays towards a given sample which generates a **diffraction pattern**. When the beam reaches the sample, it is scattered at an angle (a.k.a. the **scattering angle**) typically denoted as **2Θ** relative to the incoming beam. **Bragg's Law** describes how X-ray scattering is measured:

$$n\lambda = 2d\sin\Theta$$

In this example, n is an integer (1,2,3…), λ is the wavelength of the X-ray beam, d = the distance between repeating planes of lattice points or of atoms (specifically, the electron density of the atoms), and Θ is half of the aforementioned scattering angle.

The TGA and XPS experiments mentioned earlier in this section provide 'chemical' information, specifically stoichiometric (ligand:metal ration) and local bonding properties. However, these experiments are unable to distinguish between amorphous, polycrystalline, or single-crystal materials. Powder XRD (PXRD) is considered the best method for determining bulk crystallinity in a sample. Matching a single-crystal or PXRD spectrum to a literature spectrum is an important aspect of the technique. In this experiment, "matching" means peaks at equivalent angles (2Θ) with comparable intensities, although the 2Θ values are considered more important. Our samples match the literature values well [22]. However, the true importance of the PXRD technique for our purposes is in assessment of the degree of crystallinity, which is experimentally determined by the width of the peaks and baseline flatness – the narrower the peaks, the more crystalline the material. Figure 24 shows a literature example of a PXRD spectrum of UiO-66 from [22]. Figures 25-27 shows our experimental PXRD spectra for our UiO-6x MOFs.

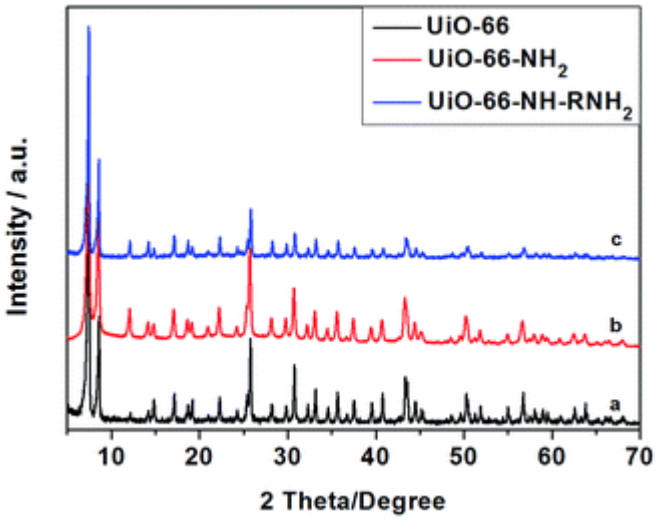

Figure 24 – Literature XRD scan of UiO-66 from [22].

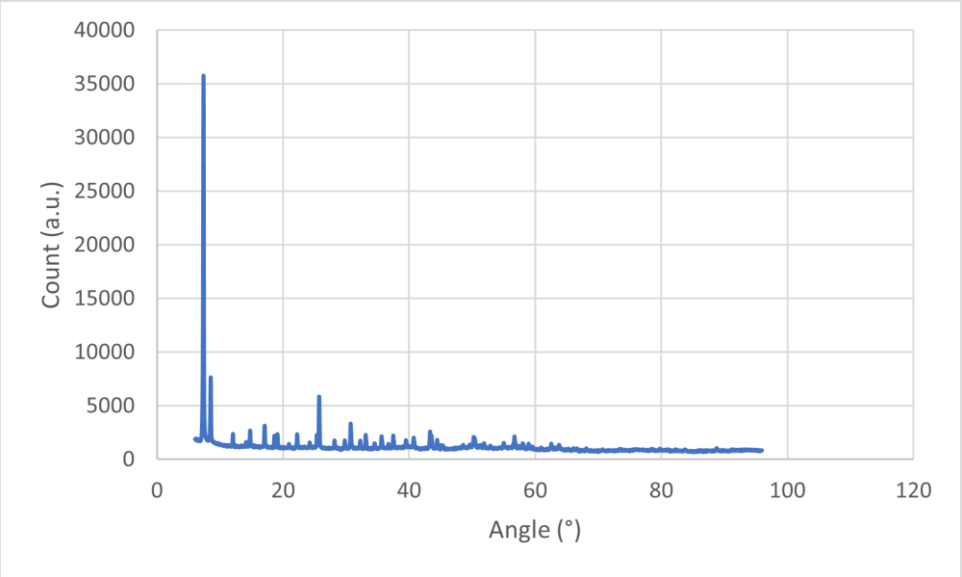

Figure 25 – PXRD scan of our UiO-66 (terephthalic acid ligand).

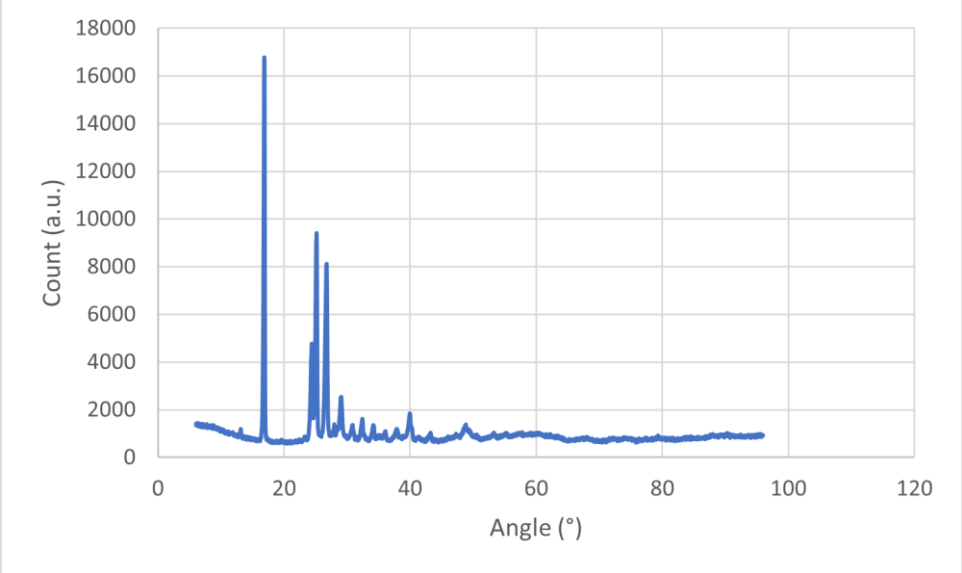

Figure 26 – PXRD scan of our UiO-67 (biphenyl dicarboxylic acid ligand).

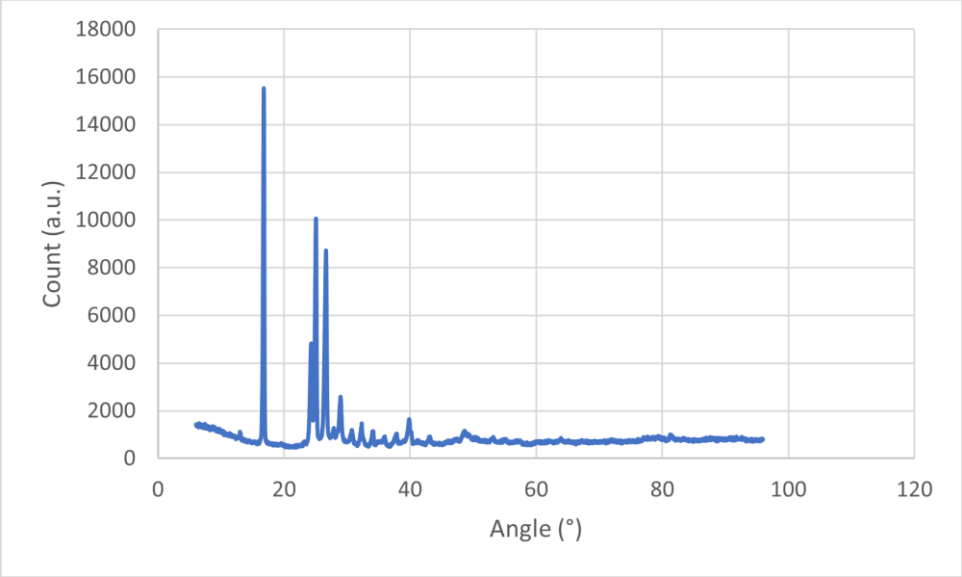

Figure 27 – PXRD scan of our UiO-67-bipy.

A full crystal structure was not derived from the data in Figures 25-27 however, it did provide insight into the crystallinity of our synthesized MOFs. Based on the narrow, sharp peaks that are present, we concluded that our reactions succeeded in creating crystalline MOFs for UiO-66, UiO-67, and UiO-67-bipy. It is also worth noting that the PXRD spectra for UiO-67 (Figure 26) and UiO-67-bipy (Figure 27) are very similar. The reason for this being that the major scatterers, the Zr-Zr and Zr-O vectors, are the same distance because the peaks are at the same 2Θ. This is one way that PXRD can give structural information in similar species – the relative sizes of the pores would be related to the cluster spacings, which can be determined from the 2Θ values. Going forward, this is one way to help characterize materials that have different-length spacers, e.g., bithiazole or furan.

2.5. Synthesis of heteroaromatic UiO-66 derivatives

Based on the reaction scheme in Figure 14, two derivatives of UiO-66 were synthesized, although not yet fully characterized. Using 2,5-thiophenedicarboxylic acid and 2,5-furandicarboxylic acid, we implemented the same reaction conditions in Figure 15 which showed good yields consistent with the expected physical appearance of the expected MOFs UiO-66-T (thiophene bridge) and UiO-66-furan (furan bridge). The latter is a new compound, previously unpublished in the literature.

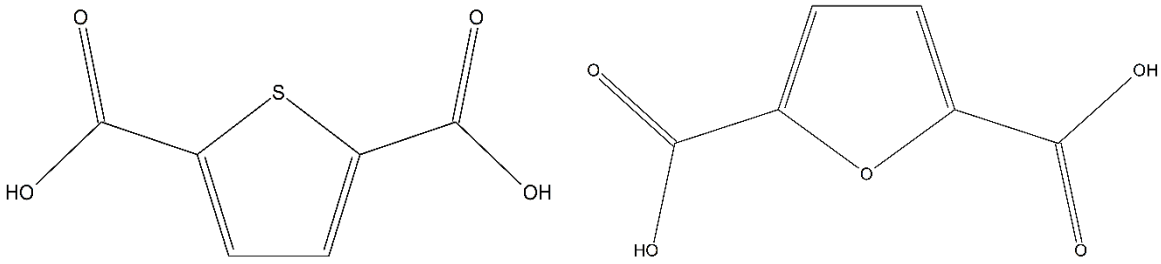

Figure 28 – Structures of 2,5-thiophenedicarboxylic acid (left) and 2,5-furandicarboxylic acid (right).

2.6. Microwave synthesis of the UiO-6x family

Near the end of this project, a microwave reactor was installed in the department, allowing us to synthesize-UiO-6x MOFs by this alternative method. Microwave radiation is a non-ionizing form of radiation and cannot break chemical bonds (other than through indirect pyrolysis). Only rotation is induced upon molecules. The microwaves are generated via a magnetron; and like all forms of electromagnetic radiation, they are made up of oscillating, orthogonal electric and magnetic fields [23]. The electric field component interacts with the molecules in a reaction vessel by way of dipolar polarization or ionic conduction. The reaction rate enhancement provided by microwave heating is the result of instantaneous localized superheating of the reaction mixture, which is governed by the Arrhenius equation [23]:

$$k = Ae^{-\frac{E_a}{RT}}$$

In this equation, k = the rate constant, A is the pre-exponential factor, E_a is the activation energy of the reaction, and RT is the average kinetic energy. This equation states that high temperatures and low activation energies will favour a larger rate constant, thus speeding up the reaction. The heating is also more uniform, taking place evenly throughout the whole reaction vessel, which generally leads to more consistent results and higher yields in addition to the vastly decreased reaction time.

Microwave-assisted synthesis presented a unique opportunity to optimize one aspect of the reaction scheme outlined in Figure 15: time [23][24]. Our solvothermal reaction conditions of 120 °C of heating over 24 hours was shortened to just 18 minutes of microwave heating.

After developing our reaction method, we were able to quickly synthesize analogues of the UiO-6x MOFs that were previously synthesized via solvothermal methods. This included UiO-66 (with 2,5-thiophenedicarboxylic acid and 2,5-furandicarboxylic acid analogues), UiO-67, and UiO-67-bipy. The characterization of some of these materials will be presented in Chapter 3.

3. Preliminary Solid-State Nuclear Magnetic Resonance Characterization

Solid-state NMR (SS-NMR) spectroscopy is a useful technique to characterize structure for solid phase samples such as powders and single crystals. Although SS-NMR is analogous to liquid-state NMR in many aspects, some complications arise with regards to spin states in SS-NMR. In traditional liquid-state NMR, many of the spin interactions are averaged out by the tumbling of the molecules in solution. In the solid-state, the **anisotropic** (i.e., property of a material to have unique properties along a given direction(s)) spin interactions remain [25]. Some of these interactions include **dipolar coupling** and **quadrupolar interactions**. Dipolar coupling is the result of the magnetic field generated by nuclear spins interacting with the dipole moment of other nuclei [26], whereas quadrupolar interactions arise from nuclei with a spin quantum number of > ½, because they have a non-spherical charge distribution with a complimentary electric quadrupole moment tensor. This nuclear quadrupole moment couples with the surrounding electric field gradients (EFG) [25][26]. These interactions typically result in greater **line broadening** for SS-NMR samples [25].

One of the fundamental techniques to achieve narrower and more intense NMR lines for better characterization is known as **magic angle spinning** (MAS). This technique works by rotating the sample at the **magic angle** ($\theta_M \sim 54.74°$) with respect to the direction of the static magnetic field of the NMR magnet to cancel or negate altogether the aforementioned anisotropic contributions. This magic angle can be derived mathematically from the nuclear dipole moment, which has a $3\cos^2\theta - 1$ dependence relative to the applied magnetic field, i.e., this term goes to zero (and along with it the anisotropic line broadening) when $3\cos^2\theta = 1$, which occurs when $\theta = \sim 54.74°$.

To completely negate these anisotropic contributions, the sample must be spun at a rate that is equal to or greater than the dipolar linewidth (with a powder sample (like the ones used in this research), using MAS to spin a rate that is slower than the largest anisotropic contribution yields an incomplete averaging of this contribution [25]). For the observed spectra, **spinning side bands** will appear in addition to standard isotropic chemical shifts unless the spinning rate is larger than the spectral window. Spinning side bands are distanced from the isotropic frequency by multiples of the magic angle spinning frequency. Although these side band frequencies can yield structural information of the material being analyzed, they are generally undesirable as they can overlap with the isotropic chemical shifts of other nuclei [25]. As a practical matter, ^{13}C nuclei on the Lakehead University solid-state instrument resonate at a frequency ~126 MHz, and the rotational speed is typically set for 10 000 Hz. This would put the spinning side bands at multiples of approximately +/- 80ppm from the isotropic chemical shifts (*i.e.*, based on (10 000 Hz / 126 000 000 Hz = 0.0000794) *(1 000 000) = 79.4 ppm). For ^{1}H, the spinning side bands would appear at multiples of +/-20 ppm and would therefore be outside the typical spectral window, which spans less than 15 ppm for this system.

3.1. ^{13}C NMR spectra for UiO-6x

For our UiO-6x MOFs, initially ^{1}H and ^{13}C SS-NMR were both conducted. Because of the small chemical shift window of ^{1}H, typically <12 ppm for organic protons, peaks are generally broad and not well resolved, which we also found for our samples. However, ^{13}C SS-NMR provided resolved spectra as well as good structural information on our MOFs, and therefore only those spectra are shown in the Figures below:

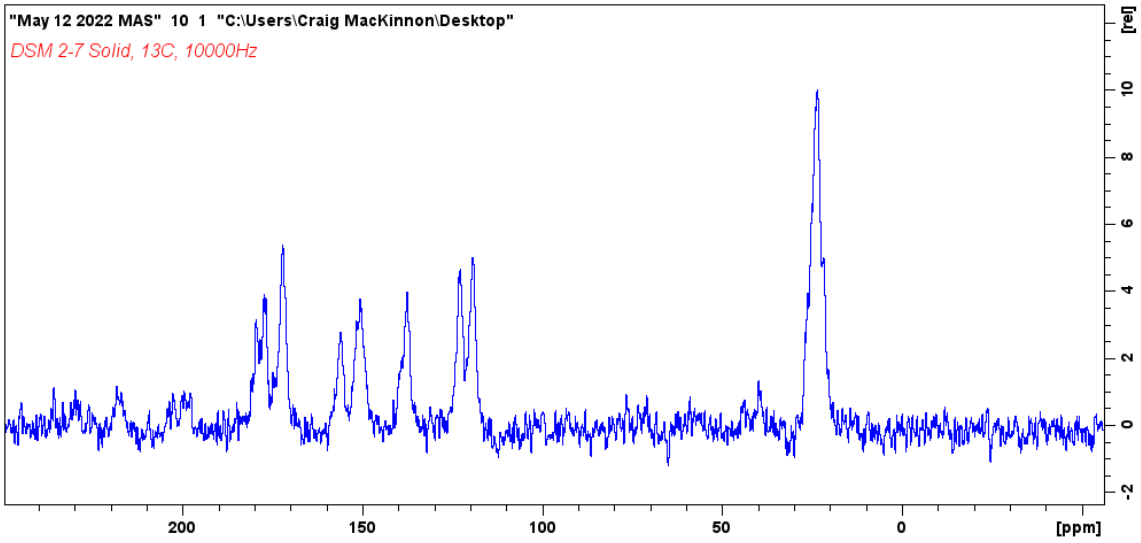

Figure 29 - ^{13}C SS-NMR spectrum for UiO-67-bipy synthesized via solvothermal methods. Peak in the 30 ppm range indicate the acetic acid modulator, phenyl carbons in the 120-150 ppm range, and the carboxylic acid carbons in the 170 ppm range.

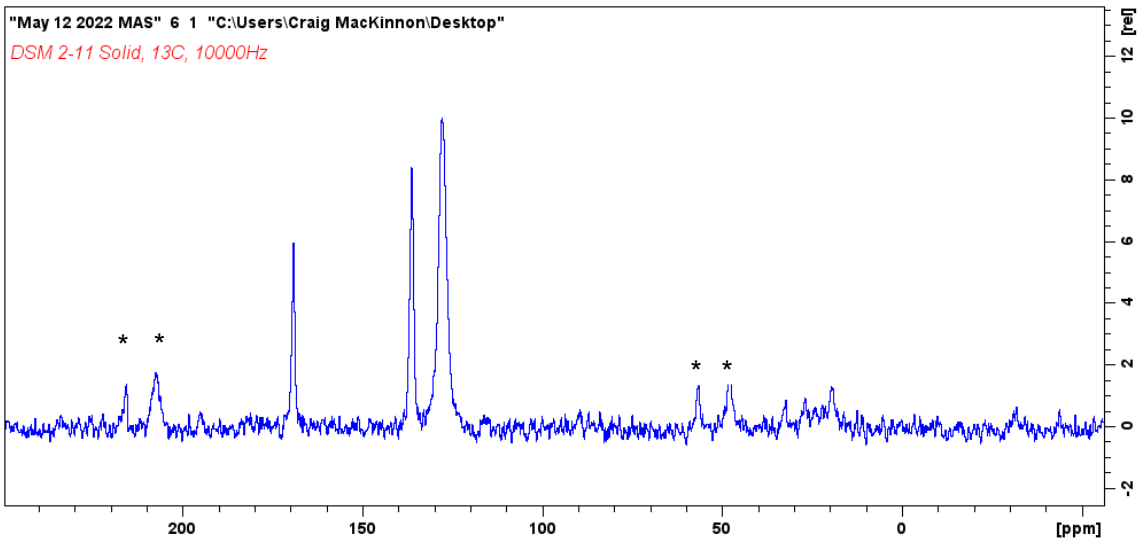

Figure 30 - ^{13}C SS-NMR spectrum for UiO-66 synthesized via solvothermal methods. Phenyl carbon peaks located at ~130 ppm followed by carbonyl-connecting carbon at ~140 ppm and carboxylic acid carbon at ~170 ppm. Minor shifts in the 30 ppm range indicate the acetic acid modulator. Peaks marked with * are spinning side bands.

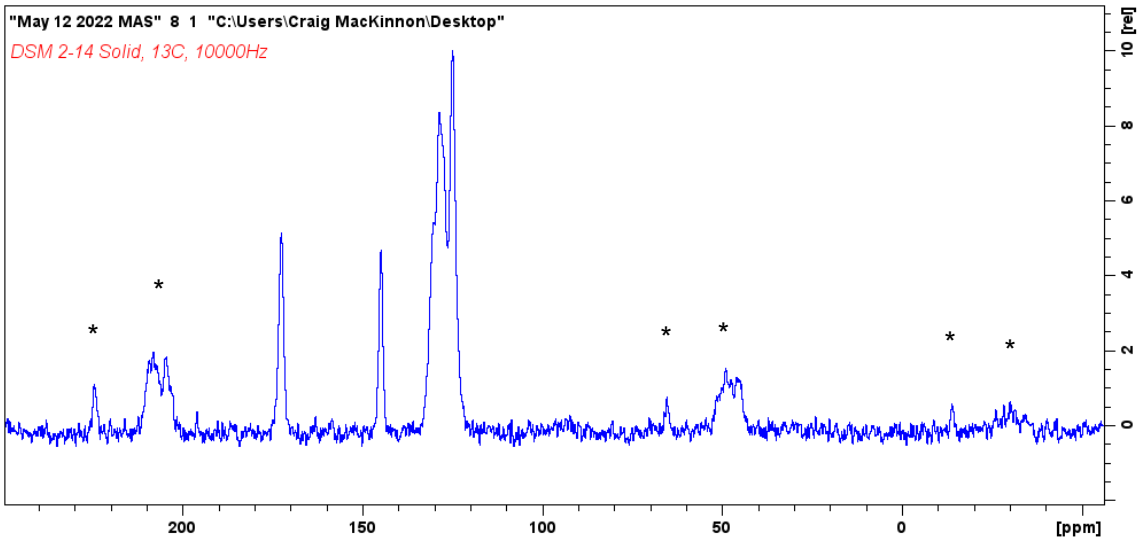

Figure 31 - ^{13}C SS-NMR spectra for our UiO-67 synthesized via microwave reactor. Phenyl carbon peaks located in the ~130 ppm range with carbonyl-connecting carbons shift at ~ 140 ppm and carbonyl carbons at 170ppm. Peaks marked with * are spinning side bands.

Figures 29-31 illustrate the ^{13}C SS-NMR spectra for our UiO-6x family of MOFs. The peaks marked with * in Figures 30 and 31 are spinning side bands. With these spectra, we were able to identify the resonances due to the organic linkers. No solvent resonances were detected, indicating that the pore spaces were completely empty. In

conjunction with the other instrumentation that was done via XPS and XRD, we were able to fully characterize our materials. We also demonstrate that the pores are indeed empty of solvent (at least, any solvent with a carbon in it) – XRD would not give this information, especially if the solvent molecules were ordered (the solvent in this case is also DMF, which gives a distinct 3-line pattern in ^{13}C NMR); there is similarly no acetone peak, which is the solvent the material was washed with. SS-NMR would also have a higher sensitivity (be able to detect solvent at a smaller amount) than XRD.

3.2. Feasibility of SS-NMR as a Characterization Technique for MOFs

Beyond the chemical shift identification, the relative sharpness of our peaks in Figures 29-31 (in conjunction with PXRD spectra) also suggests that our materials are crystalline in nature. One thing that can be identified in Figures 29 and 30 compared to their corresponding PXRD spectra is the presence of the acetic acid modulator. At roughly ~30 ppm the resonance is clearly evident for UiO-67-bipy (Figure 29) and less so for our UiO-66 (Figure 30). This peak is distinctly absent from our UiO-67 synthesized via microwave (Figure 31), however. One possible reason for the lesser amount in the latter is that there is not a significant amount of the modulator left on the surface of the material to be identified via SS-NMR. A more idealistic assumption is that the lack of acetic acid in the case of Figure 31 is the result of a more crystalline material. The acetic acid that remains post-workup acts as a “band-aid” for any remaining Zr bonds not linked to a carboxyl group from our diacids, so if the crystal is internally perfect, one acetic acid group would be present for every available metal node on the external surface of the MOF, which would become a negligible amount compared to the ligand carboxyl groups for large crystallite sizes, leaving them lost in the baseline of our spectrum.

Another important conclusion drawn from Figure 31 is how well resolved the spectrum is for UiO-67 synthesized via microwave-assisted methods. This shows promise that using this faster and more efficient technique will yield crystalline material comparable to or better than the best produced by solvothermal methods.

One problem with SS-NMR is that the wider peaks can hide or combine with additional peaks, making the separate peaks unresolvable. One way to check if this is the case is to run spectra on instruments of different field strengths. To this end, UiO-66 was synthesized via solvothermal methods and analyzed on the SS-NMR spectrometer (14.2T) of the Charlottetown Research and Development Centre (Figure 32).

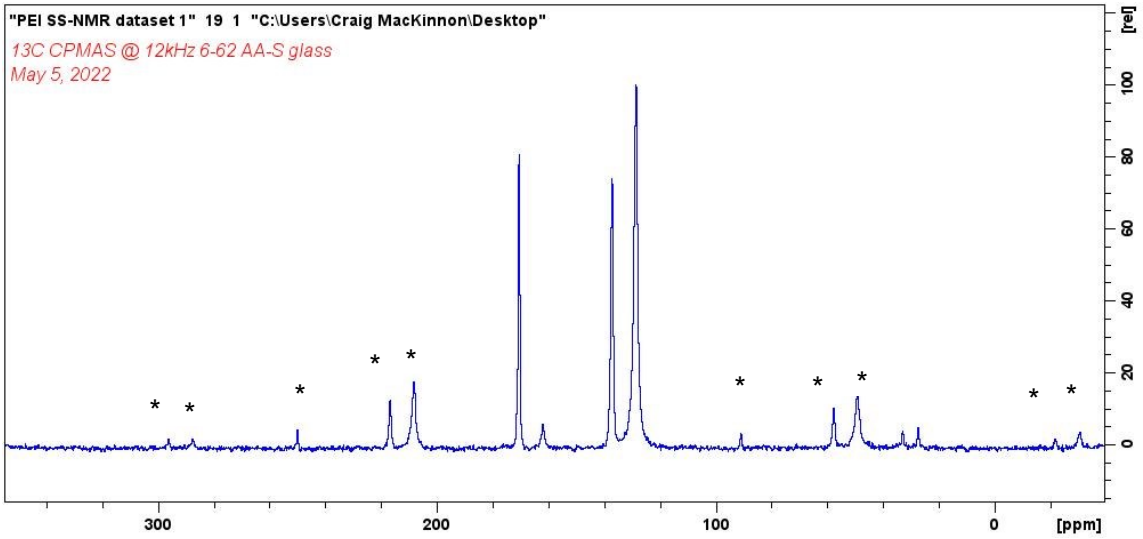

Figure 32 – ^{13}C NMR spectrum of UiO-66 synthesized via solvothermal methods acquired at the University of PEI. Phenyl carbon peaks located at ~130 ppm followed by carbonyl-connecting carbon at ~140 ppm and carboxylic acid carbon at ~170 ppm. DMF solvent peaks are present at 27, 33 and 162 ppm. Peaks marked with * are spinning side bands.

It is notable that DMF peaks can be seen in this spectrum. The washing/drying and activating process of these MOFs was apparently not as rigorous as was used with the Thunder Bay samples. This highlights the importance of thoroughly drying/pumping samples prior to collecting spectra.

The MAS spin rate for the Charlottetown Research and Development Centre's SS-NMR was 12kHz, which yields similar spinning side-bands for ^{13}C at ~80 ppm, which are denoted by *. Directly comparing Figures 30 and 32 however, it is plain to see the similarities in the chemical shifts. All of the key isotropic peaks for our terephthalic acid ligand are noted in both Figures 30 and 32. That being said, we can validate Lakehead's instrument as being appropriate for our purposes.

Another spectrum that was collected via the Charlottetown Research and Development Centre's SS-NMR was related to the degradation of the organophosphate pesticide glyphosate by UiO-66 (the results of similar testing are shown in Chapter's 4 and 5). ^{13}C SS-NMR spectra were collected UiO-66, UiO-66 solid after being suspended in an aqueous solution (1:1 mass ratio of MOF: pesticide) with glyphosate, and glyphosate by itself. The SS-NMR spectra for these different tests are shown in Figure 33:

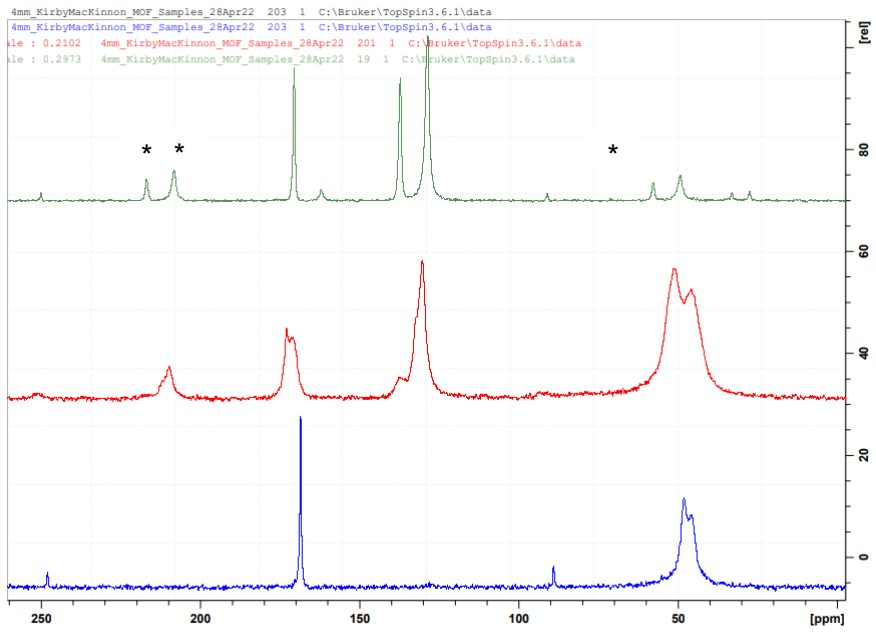

Figure 33 – ^{13}C SS-NMR spectra of UiO-66 (top, green), UiO-66 after suspension in water in the presence of glyphosate (middle, red), and glyphosate (bottom, blue). Phenyl carbon peaks located at ~130 ppm followed by carbonyl-connecting carbon at ~140ppm and carboxylic acid carbon at ~170 ppm for the top and middle lines. DMF solvent peaks are present at 27, 33 and 162 ppm. Peaks marked with a * are spinning side bands.

The top (green) and bottom (blue) spectra are the starting materials UiO-66 and glyphosate, respectively. The middle (red) spectrum is the result of stirring the two materials together with each other in water for several hours. The product was then washed and dried – the washing process would remove any unreacted glyphosate, which is soluble in water. As can be seen from the middle (red) spectrum, peaks from both the UiO-66 and glyphosate remain. Judging from the comprehensive rearrangement of the original UiO-66 resonances, it can be concluded that the pore environment has completely changed, i.e., that the cavities are completely occupied, presumably by glyphosate.

4. GC Degradation Testing

One significant use for the UiO-6x family is the degradation and/or sequestration of phosphate-based molecules, as discussed in Chapter 1. Due to ease of availability, dimethyl methylphosphonate (DMMP) was chosen as the first target compound for hydrolysis by our MOFS. DMMP is an organophosphorus CWA simulant compound that is a less toxic analogue to the G-series of nerve agents.

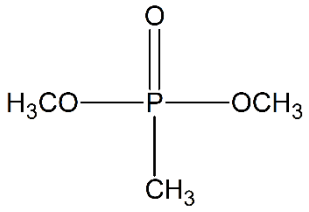

Figure 34 – Structure of dimethyl methylphosphonate (DMMP).

Rodrigo et al. [8] explored gas chromatography to monitor the ability of UiO-66 to break down diisopropylfluorophosphate (DIFP) in an aqueous environment. As most CWA simulants are relatively volatile, GC is an easy way to monitor reaction progress via small aliquots taken from the reaction vessel.

For our degradation testing, we measured the loss of DMMP by its decrease in signal via its GC chromatogram. Literature results would suggest that DMMP would break down in the presence of UiO-6x MOFs [8], however, there is the possibility that it could be sequestered whole into the MOF. A GC method was developed, which is reported in Chapter 7 (experimental methods). UiO-66 and UiO-67 showed little to no reaction with DMMP, which correlates well with literature results [27]. However, UiO-67-bipy was uniquely shown to break-down/sequester DMMP in an aqueous environment over the course of 90 minutes: Whether this result indicates the decomposition or sequestration

will have to be resolves by SS-NMR, which requires reaction scales that are orders of magnitude larger than these GC trials.

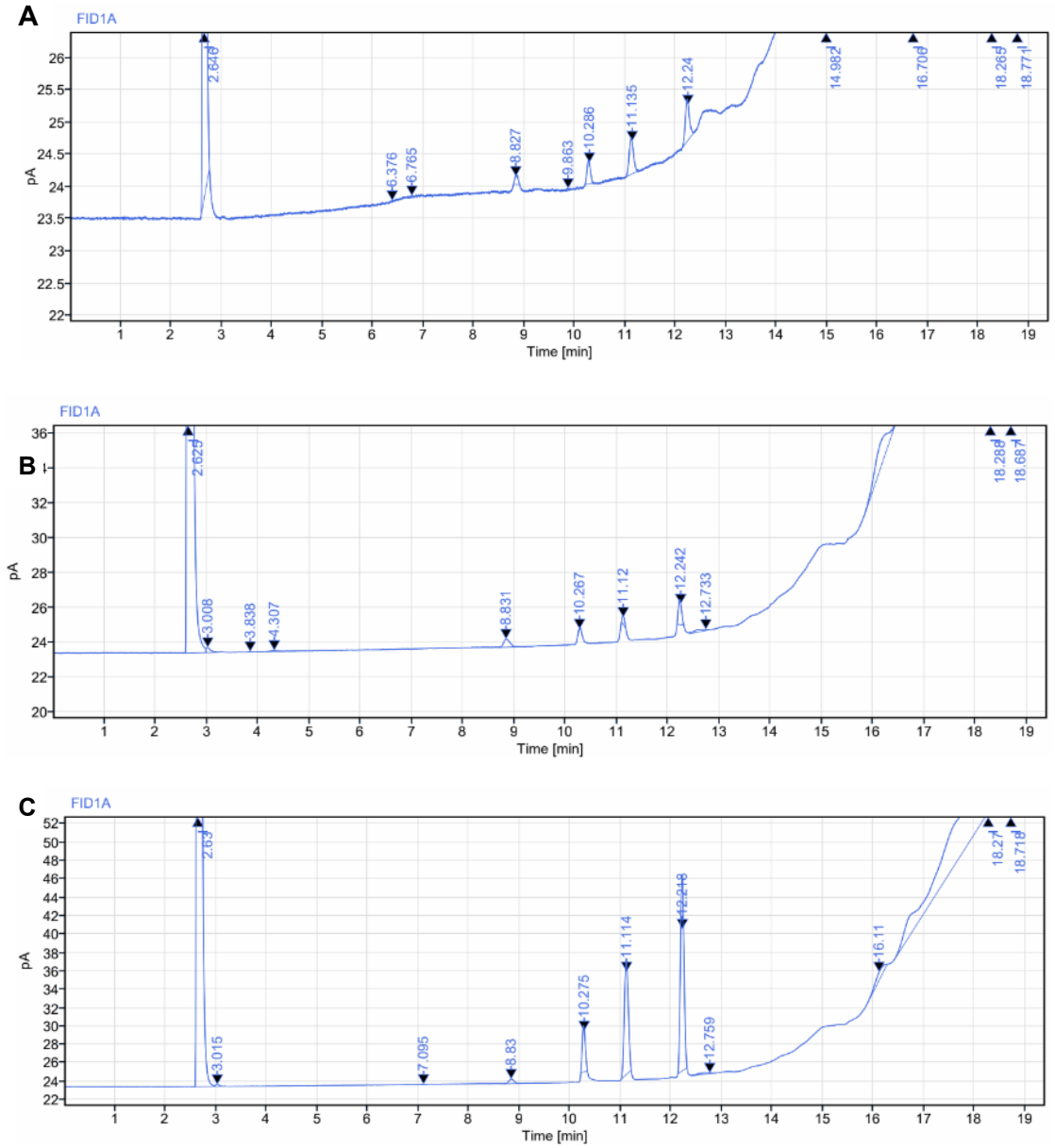

Figure 35 – Chromatograms of the degradation of DMMP by UiO-67-bipy after 30 (a), 60 (b) and 90 (c) minutes. DMSO peak is at ~12.2 minutes and DMMP peak is at ~11.1 minutes.

Table 2 – Summary of GC chromatogram data for UiO-67-bipy with calculated peak area ratios

Time	DMMP area	DMSO area	Ratio of DMMP/DMSO
30 min	3.29	3.61	0.911
60 min	68.62	104.67	0.656
90 min	1.63	6.28	0.259

The chromatograms highlighted in Figure 35 and the data within them summarized in Table 2 highlight the removal from solution of DMMP by UiO-67-bipy over the span of 90 minutes. Although we did not see the same results for UiO-66 and UiO-67 as expected [20] (we will continue to test these materials as “base compounds” in our subsequent experiments (as reported in Chapter 5)).

When turning to pesticides, GC is not an appropriate method for following reasons. Pesticides have much lower vapour pressures and would not be easily volatilized in a GC experiment. Therefore, we turned to HPLC, as documented in the next chapter.

5. HPLC Analysis of Organophosphate Degradation

The organophosphate molecules that were investigated are dimethoate, (2-chloroethyl) phosphonic acid, glufosinate ammonium, glyphosate, malathion, and methyl paraoxon. All of these compounds are organophosphates with at least some similar chemical features to DMMP and previously tested CWAs. They are also commercially available in pure form and relatively inexpensive. Most importantly, these compounds are of current interest with regards to their use in agriculture.

As mentioned, GC is not an appropriate method for testing these materials, at least with the equipment available at Lakehead University. Within the operating parameters (specifically the max temperature of the column) of the GC, these pesticides did not elute. Therefore, an analogous reaction setup which incorporated the use of high-performance liquid chromatography (HPLC) to monitor reaction progress was developed.

To analyze the potential degradation of organophosphorus-based pesticides by our MOFs, reaction conditions similar to those described in Chapter 4 were used. Based on analytical standard testing reported by Harshit et al. [28] on organophosphate compounds, an HPLC method was adapted for our purposes. Unfortunately, even working with a well-adapted HPLC method, resolution between our DMSO internal standard and our organophosphorus-based pesticides proved to be challenging. Of the 6 standards that were analyzed, only 3 provided moderately good resolution even after troubleshooting our HPLC method extensively. Thus, these three were chosen for the actual degradation testing: (2-chloroethyl) phosphonic acid, malathion, and methyl paraoxon (shown below in Figure 36).

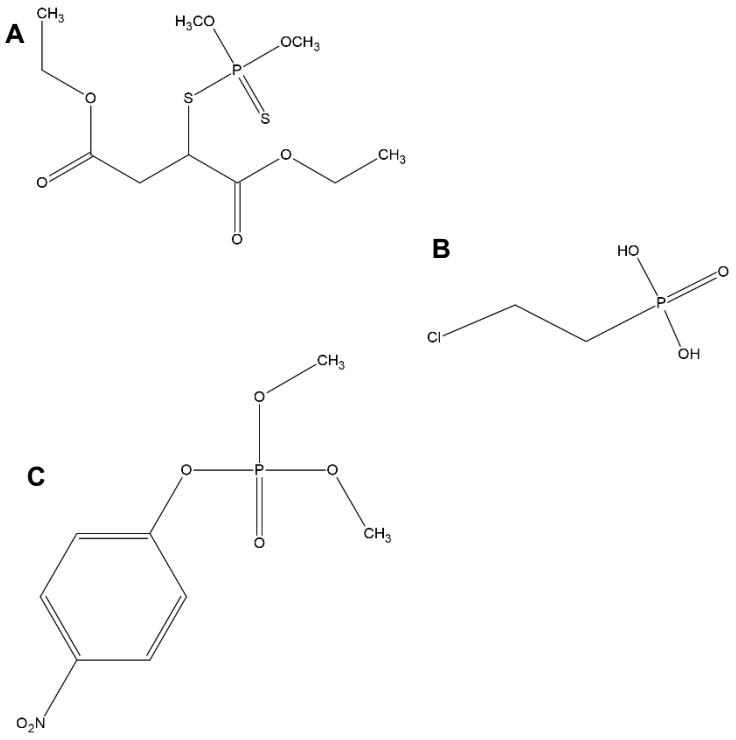

Figure 36 – Structures of malathion (a), (2-chloroethyl) phosphonic acid (b), and methyl paraoxon (c).

In a similar fashion to our GC degradation testing, an aqueous environment with our MOF, DMSO internal standard and now our chosen organophosphorus-based pesticide was established. Two of the three pesticides, malathion and methyl paraoxon, exhibited no loss of material (either through sequestration or hydrolytic decomposition) with any of our MOFs. By contrast, (2-chloroethyl) phosphonic acid was partially degraded/sequestered by UiO-67 but not by UiO-66 or UiO-67-bipy.

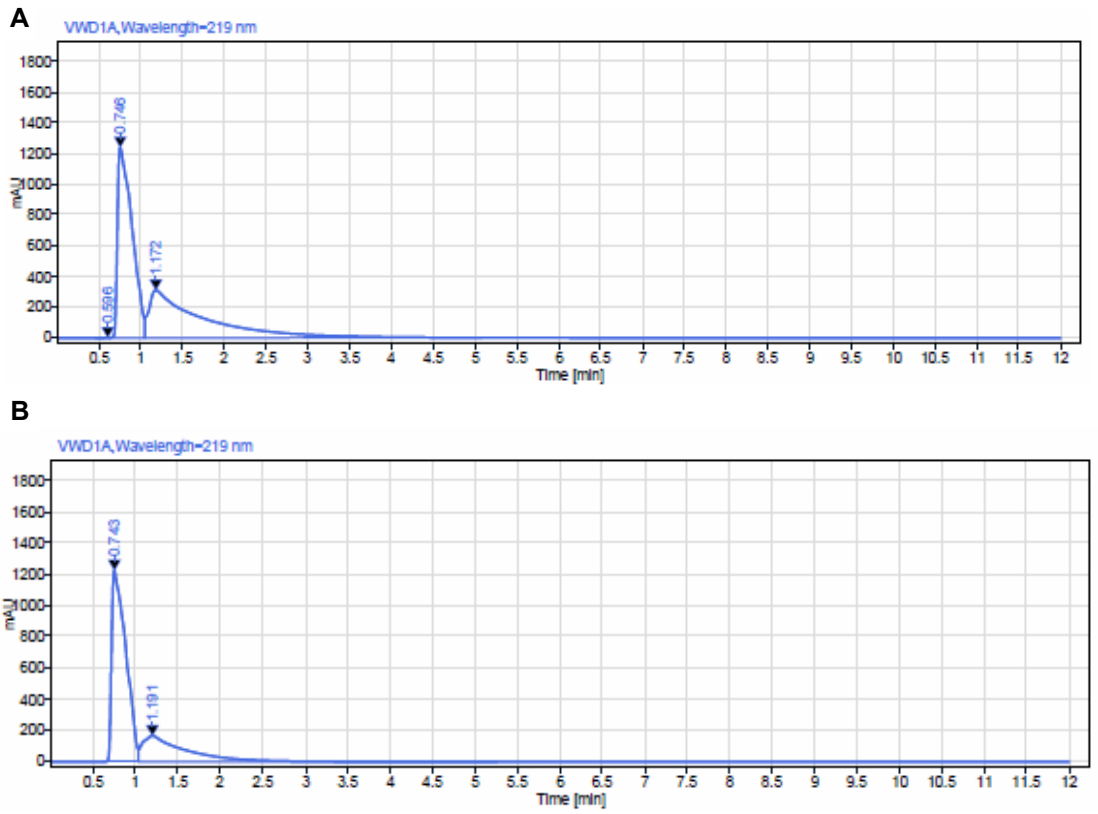

Figure 37 – HPLC chromatogram of the degradation of (2-chloroethyl) phosphonic acid by UiO-67 after 1 hour (a) and 4 hours (b). The retention time of ~ 0.74 minutes is DMSO and the retention time of ~1.18 minutes is (2-chloroethyl) phosphonic acid.

Table 3 – Summary of HPLC chromatogram for UiO-67 data with calculated peak area ratios

Time	(2-chloroethyl) phosphonic acid area	DMSO area	Ratio of (2-chloroethyl) phosphonic acid /DMSO
1 hour	13921.17	15035.57	0.926
4 hours	6072.88	14177.81	0.428

As shown in Figure 37 and summarized in Table 3, the amount of (2-chloroethyl) phosphonic acid was reduced by nearly half after of 4 hours of exposure to UiO-67, but no further interaction was detected after 24 hours of exposure. As mentioned for our GC results in Chapter 4, it cannot be said for certain if the (2-chloroethyl) phosphonic

acid is being degraded or adsorbed by our MOF. If the latter, it is possible that a certain “adsorption capacity” for UiO-67 was reached and it could not accommodate any further (2-chloroethyl) phosphonic acid or any of its potential degradation products. Another possibility is that UiO-67 reacts stoichiometrically with (2-chloroethyl) phosphonic acid and the MOF was completely destroyed by the time 4 hours had passed.

Although this was a promising result, it was not necessarily expected that UiO-67 would be the only MOF to show any sort of ability to degrade these pesticides under these specific conditions. With UiO-67-bipy showing the unique ability to degrade DMMP under similar conditions, it was expected that UiO-67-bipy would be more likely to react with pesticides, rather than the base UiO-67. This was not the case under our testing parameters, however. The results given in Chapters 4 and 5 show that we have an incomplete understanding of what is happening in the interaction between the MOFs and the organophosphate compounds. There is no obvious reason to suggest why UiO-67-bipy would react with only DMMP while UiO-67 is the only MOF that reacts with (2-chloroethyl) phosphonic acid. Exploring these materials post reaction via SS-NMR could provide valuable insight.

6. Summary, Conclusion, and Future Work

6.1. MOF synthesis methods

For generating MOFs, it is known that the method of synthesis can greatly affect the crystallinity and activity of the material. To this end, we have found general solvothermal and microwave-assisted synthesis methods that yield good uniformity, reproducibility and activity. The reaction conditions that we finalized for both methods are general and appear to function for any aromatic diacid organic linker. With little differences between the solvothermal/microwave products, the shorter reaction times of the microwave method are more promising with the caveat being needing a microwave reactor. For both methods, acetic acid was verified as a suitable modulator for all reactions conducted.

As our reaction conditions worked equally well for UiO-66, UiO-67 and UiO-67-bipy, for future work in developing new MOFs, we could apply this template to mixed MOFs. Mixed MOFs have alternating or multiple different types of metal nodes and/or organic linkers. Their use is an emerging field which has shown promise in some of the traditional MOF applications such as gas storage, gas separation, and as chemical sensors [27][29]. For the purposes of this research, incorporating the use of multiple ligands in one MOF is an idea to increase the functionality of our materials based on the results outlined in sections 4 and 5. With the largest of our ligands showing the most promise (UiO-67) for degrading organophosphates, it can be extrapolated that the nucleophilicity of UiO-67-bipy and size of UiO-67 are key factors in their functionality. Incorporation of even larger ligands such as that found in UiO-68 with additional functionalization provided by heteroaromatic ligands without the loss of pore size are likely candidates for further degradation testing.

6.2. **Characterization of UiO-6x MOFs**

Characterization of MOFs generally requires a combination of instrumental methods that each give only a partial picture of the material. Therefore, it can be a challenge to combine the evidence from the various methods into a cohesive picture of the MOF. For example, TGA analysis is straightforward but provides limited structural information. Therefore, our staple techniques especially going forward will be XPS, XRD, and SS-NMR.

Through XPS data we were able to establish key bonding environments within our material. Beyond establishing that Zr oxide metal clusters were being generated, it also demonstrated (for the C 1s region), how much our ligands were involved in the coordination environment with the Zr nodes. As demonstrated in Section 2.4., the lack of free COOH character indicates that most of our carboxylate substituents are coordinated to Zr nodes. For future characterizations using XPS, we hope to have our own deconvoluted spectra to further establish the coordination environment within our materials.

Powder XRD proved to be another useful tool in this research. PXRD gave us a good measure of the crystallinity of our material. This technique proves that our materials are indeed MOFs with an extended crystalline structure, rather than simply a mixture of molecular coordination complexes. The sharp peaks in our PXRD spectra outlined in section 2.5. prove good crystallinity for our MOFs. The spectra are primarily dependent on the spacing of the zirconium-oxide nodes, however, and so there is little difference between MOFs with same-sized spacers. This is clearly seen when comparing the spectra for UiO-67 and UiO-67-bipy.

Unfortunately, installation and commissioning of Lakehead's new SS-NMR instrument was only finished late in the project. As a result, time on the instrument was limited and with only one rotor available, sample preparation was a slow process. Therefore, the data presented herein is only preliminary, although it is very promising. As outlined in Chapter 3, ^{13}C NMR data were obtained for several MOF samples. The spectra we obtained show that we can use SS-NMR to be able to characterize our organic ligands within the MOFs successfully. For at least UiO-66 and -67, the peaks are quite narrow. Although it will take additional experiments to prove beyond a reasonable doubt, narrow line widths in the SS-NMR correlate with narrow peaks in the PXRD, suggesting that SS-NMR might be a useful technique to also characterize crystallinity. We also note that the 126 MHz ^{13}C solid-state spectrum shows ample resolution. Running the same materials at 151 MHz does not reveal any overlapping peaks (as we expected). For future work using SS-NMR, we hope to incorporate its use in characterizing our heteroaromatic UiO-66 MOFs, as well exploring some other spin active nuclei such as ^{1}H (which was attempted, but we did not achieve well resolved spectra) and ^{31}P on post-reaction samples to determine the fate and chemical structure of the phosphorus that originated in the pesticide substrate.

6.3. **Reaction of organophosphates as followed by GC and HPLC**

In order to screen for potentially interesting chemistry between MOFs and organophosphates, we first worked with UiO-style MOFs, namely UiO-66, -67, and-67-bipy. We followed the reaction by GC or HPLC depending on the nature of the organophosphate – GC is easier and faster, but obviously only works for compounds with a low enough boiling point. As described in Section 4, our GC testing was based off work done by Rodrigo et. al [8]. Although those authors looked at the CWA simulant diisopropyl fluorophosphate (DIFP), we used the more accessible dimethyl methylphosphonate (DMMP), which has itself been used in some studies as a G-series nerve-gas substitute. Ultimately, DMMP was only noted to be degraded or sequestered by our UiO-67-bipy MOF. With fixed amounts of both DMSO (internal standard) and DMMP, we noted the relative peak area ratio decrease outlined in section 3 and summarized in Table 2. We tested the aforementioned UiO-6x MOFs synthesized via solvothermal and microwave-assisted methods, both leading to similar results. The expected mechanism of action for UiO-67-bipy to degrade DMMP is outlined in Section 1.7. where small organophosphates are likely to be broken down via hydrolysis [8][15].

As previously noted, for volatile CWA simulants, specifically DMMP in our case, GC testing was viable. However, our GC column temperatures could not exceed roughly 250 °C, which in practice, was insufficient to volatilize most organophosphate pesticides. Therefore, an HPLC method was developed to monitor the potential degradation of these pesticides in an aqueous solution. A previously published HPLC method that was used to monitor organophosphorus pesticides [28] analytically was adapted for our purposes. The exact parameters used by this research group gave poor resolution with our DMSO standard, so the solvent composition and flow rate were modified. Six agrichemicals were available, namely: dimethoate, (2-chloroethyl)

phosphonic acid, glyphosate, glufosinate ammonium, malathion, and methyl paraoxon. As mentioned in Chapter 5, these organophosphates were of specific interest due to their ongoing use in agriculture [13]. Glyphosate has been shown to be partially adsorbed to the surface of UiO-67 and **paraoxon**, the metabolite of the insecticide **parathion** has been shown to be sensed by MOF-5, a Zn metal-based MOF [29]. However, the fact that these compounds in relation to their degradation and/or sequestration by MOFs is not well documented as whole makes them good choices for our work.

Of the 6, only 3, (2-chloroethy) phosphonic acid, malathion, and methyl paraoxon yielded passable chromatograms for standards testing. This was after modifications to the method were made, which included a solvent ratio of 30/70 by volume of water to acetonitrile (up from 10/90) and increased mobile phase flow rate of 1.0 mL/min (up from 0.75 mL/min). After developing a suitable method for these 3 compounds, degradation testing was done. The use of a DMSO internal standard was once again used for simplicity. As detailed in section 5, two of these pesticides did not seem to interact with any of the tested MOFs. One promising result is described, however, with the partial degradation of (2-chloroethyl) phosphonic acid by UiO-67. This was unexpected, as UiO-67 did not show any degradation ability with DMMP, where as UiO-67-bipy did. UiO-67-bipy was expected to have a higher reactivity when compared to regular UiO-67 due to its nucleophilic nitrogen atoms located within the ring system. This relates back to work done by Rodrigo et al. with UiO-66-NH_2 where they showed this amine-functionalized MOF had increased reactivity compared to its unsubstituted counterparts. For UiO-67-bipy, there is a chance due to the aqueous environment that water molecules are hydrogen bonding into the pores of the MOF, preventing further reactions with any potential guest molecules. Gas-phase experiments might yield more

promising results for these materials. It is predicted that UiO-67 demonstrated slight reactivity simply based on the pore size of the MOF, i.e., it showcased an ability to adsorb (2-chloroethyl) phosphonic acid within itself. This adsorption and not degradation/hydrolysis is predicted as the mechanism of action as even after 24 hours, some (2-chloroethyl) phosphonic acid remained in solution.

Malathion and methyl paraoxon are comparatively large molecules, which is potentially one of the reasons why they were not degraded/adsorbed by our MOFs. The three pesticides that were not tested due to time constraints, dimethoate, glyphosate, and glufosinate ammonium are all relatively similar in size (smaller than malathion or ethyl paraoxon). Therefore, it cannot be said what reactivity (if any) they would have with our MOFs.

As a continuation of this chromatography testing, should more CWA simulants like DMMP be examined for degradation testing, GC is a good choice based on simplicity. However, it is very likely that HPLC will be required to measure organophosphorus-based pesticides due to their volatility. Based on the chromatograms in Figure 39, it is obvious some overlap occurred between our DMSO peak and pesticide peak ((2-chloroethyl) phosphonic acid in this case). Therefore, to make accurate determinations on how much of a given pesticide is degraded/adsorbed by our MOFs in future, a calibration curve with known amounts of these organophosphates would need to be created in favour of the existing method. Also, as all 6 of the organophosphorus-based pesticides were chosen based on their structure and relevance, continuing this testing would involve a modification of the existing HPLC method or changing the standard to accommodate for the 3 pesticides that did not get resolved.

6.4. Concluding remarks

To summarize, our goal in this research was to investigate UiO-6x type MOFs for use in agrichemistry. We also attempted to follow the reaction through all its stages and understand the MOF and the pesticide's structures through the process. Specifically, we set out to synthesize the well known UiO-66 and UiO-67, as well as the less-well-known UiO-67-bipy. Two synthesis methods were specifically compared: solvothermal and microwave assisted. Both methods yielded quality MOFs, with the microwave-assisted method being able to cut down on reaction times significantly.

Several solid-state characterization methods were used to identify our material(s) including TGA, XPS, PXRD and SS-NMR spectroscopy. A strong emphasis was placed on the use of PXRD and SS-NMR. PXRD was able to determine the degree of crystallinity present in our materials through the sharpness of the peaks. Through SS-NMR spectra we were also able to assess crystallinity based on the sharpness (or not) of our chemical shifts while also being able to derive key information about the organic ligands within our MOFs.

Beyond material characterization, the MacKinnon group hopes to use SS-NMR to characterize our MOFs post-degradation testing to fully identify which mechanisms are being used to either degrade or adsorb organophosphorous-based CWA simulants and pesticides. Using the other solid-state techniques will also be crucial to identify new MOFs (specifically the heteroaromatic analogues of UiO-66 that were not fully characterized during this project).

Using the UiO-6x family of MOFs to detoxify and/or adsorb organophosphate-based CWA simulants and pesticides was also examined via different chromatography methods. In this work, we reported the unique ability of UiO-67-bipy to

degrade/sequester a known CWA simulant, dimethyl methylphosphonate (DMMP) over the course of 90 minutes in an aqueous environment based on the method of internal standards. Several organophosphate-based pesticides were also tested against our MOFs in an aqueous environment. These “pesticides” were chosen based on their relevance and use in Canada, noting that these organophosphates are sorely neglected or even on-existent in current literature. Testing our materials showed that UiO-67 was able to partially degrade and or adsorb the growth inhibitor (2-chloroethyl) phosphonic acid over the course of 4 hours. Further reactivity with this organophosphate was not noted after this time, which is suspected to be the result of reaching an “adsorption limit” at that point in the reaction. Limited reactivity with other MOF/pesticide combinations was observed, however.

Improvements can be made to the methodology as well. For volatile CWA simulants, gas chromatography proved to be reliable, however, for all pesticides testing, HPLC was used due to the relatively low volatility of the compounds tested. HPLC chromatograms were difficult to resolve with respect to the internal standard being used, in this case, DMSO. Due to time constraints in this project, a better standard could not be found, therefore, in future work, determining a better internal standard will be crucial to establishing the reactivity of other organophosphate-based pesticides with our MOFs.

In closing, this exploratory project is merely the tip of the iceberg when it comes to exploring the reactivity of MOFs and pesticides. As mentioned, compared to CWAs, the degradation/sequestration of pesticides is poorly documented in the literature. This leaves a large opportunity for further research in this area. On top of this, there is also the fact that the UiO-6x and other MOFs are not necessarily limited to simply degrading/sequestering pesticides, with other potential applications in the form of slow-

release pesticides, personal protective equipment (PPE), and chemical sensors, to name a few [11][30][31]. This project paves the way for future work in creating materials for these important applications.

7. EXPERIMENTAL

All new reagents for MOF synthesis were purchases through Sigma-Aldrich. Organophosphate pesticides and active ingredients were purchased through Sigma-Aldrich and Toronto Research Chemicals. Synthesized MOFs were dried under vacuum and P_2O_5 before instrumentation was conducted.

TGA/DSC analysis was performed on a Netzch STA 449 F3 Jupiter Simultaneous Thermal Analyzer (STA/TGA – DSC).

XRD spectra were collected on the Pananalytical Expert Pro Diffractometer using a Pixcel detector and Anton Parr TCU 1000N Temp Control in the Lakehead University Instrument Laboratory (LUIL).

XPS spectra were collected on a Kratos AXIS Supra X-ray Photoelectron Spectrometer through the LUIL. Al anode (Kα - 1486.7 eV) was used as a monochromatic source with a 500 mm Rowland circle Monochromator

GC chromatograms were collected on an Agilent Technologies 6850 Network GC System. Column type was an Agilent J&W GC Columns DB-WAXETR with a length of 30 m, diameter of 0.320 mm, and film width of 0.25 µm.

HPLC chromatograms were collected on an Agilent Technologies 1200 Series HPLC. Column type was an Agilent InfinityLab Poroshell 120 EX-C18 (3.0 x 150 mm, 4-micron). SS-NMR spectra were collected on a 500 MHz Bruker Avance NEO Liquid and Solid-State NMR Spectrometer.

Solvothermal synthesis of UiO-6x (Sections 2.1, 2.6)

1 equivalent (281 mg, 1.204mmol) $ZrCl_4$ and 1 equivalent of organic ligand (terephthalic acid – 200 mg, 1.204mmol**;** 4,4'-biphenyldicarboxylic acid, 2,2'-bipyridine-5,5'-dicarboxylic acid, 2,5-thiophenedicarboxylic acid and 2,5-furandicarboxylic acid) were added to a 50 mL round bottom flask containing DMF and GAA (10 mL each). The solution was then sonicated for 20 minutes. During this time, a sand bath was brought to 120 °C. After sonication period, flask was placed in the sand bath and left for 24 hours (with stirring). Following the heating period, the solution was allowed to cool to room temperature. White microcrystalline powder was collected via glass filter frit and rinsed with 2 x 10 mL DMF and 2 x 10 mL acetone. Before characterization, powder was dried under vacuum with P_2O_5 (212 mg/63% yield for UiO-66).

Microwave synthesis of UiO-6x (Section 2.7)

Microwave-assisted syntheses were performed on a CEM Discover 2.0 Microwave Synthesizer.

Analogous synthetic method to the above solvothermal method was developed through the CEM software. Identical reagents and solvent amounts from the solvothermal method were added to a 35 mL Pyrex reaction flask. Microwave method was as follows: 10-minute pre-stirring phase followed by a 10 °C/min ramp to 120 °C which was held for 18.5 minutes. Cool down phase to room temperature was followed by collection of white microcrystalline powder via glass filter frit and rinsed with 2 x 10 mL DMF and 2 x 10 mL acetone. Before characterization, powder was dried under vacuum with P_2O_5.

GC Degradation testing of UiO-6x (Section 4)

Testing was done on a microscale. 0.5 mL of distilled C to a 5 mL reaction vial. 20 mg of UiO-6x was then suspended in the water. With stirring, 2.5 µL of DMSO was added as the internal standard followed by 2.5 µL of DMMP. An initial aliquot of 0.2 µL was taken for GC analysis. Subsequent aliquots were taken every 30 minutes.

GC method parameters were as follows: Initial temperature of 60 °C was held for 3 minutes followed by a 10 °C/min ramp up to 220 °C. FID detector was used and was set to 300 °C.

HPLC Analysis of Organophosphate Degradation (Section 5)

Testing was done in a 25 mL round bottom flask due to the increased sample volume required for HPLC testing. 10 mL of distilled H_2O was added to the 25 mL round bottom flask followed by 50 mg of UiO-6x. With stirring, 50 µL of the DMSO internal standard was added followed by 20 mg/20 µL for solid/liquid pesticides. An initial aliquot of 0.5 mL was taken at the start, followed by 0.5 mL every hour after the start of the reaction.

HPLC method parameters were as follows: 2 x 40 µL injections were taken from the 0.5 mL aliquots. Solvent mixture was set to a 30/70 ratio of water to acetonitrile with a flow rate of 1.0 mL/min. UV/VIS detector was set to 219 nm. Total runtime was 10 minutes with 1-minute post-run.

8. REFERENCES

1. Pfennig, B. W. (2015). *Principles of Inorganic Chemistry*. Wiley.
2. Yang, W.-yu, Chen, L., & Wang, S. (2000). Syntheses, crystal structures, and luminescent properties of novel layered lanthanide sulfonate-phosphonates. *Inorg. Chem.*, *40*(3), 507–515. https://doi.org/10.1021/ic049376u.s001
3. Hoskins, B. F., & Robson, R. (1990). Design and construction of a new class of scaffolding-like materials comprising infinite polymeric frameworks of 3D-linked molecular rods. A reappraisal of the zinc cyanide and cadmium cyanide structures and the synthesis and structure of the diamond-related frameworks [n(ch3)4][cuiznii(cn)4] and cui[4,4',4'',4'''-tetracyanotetraphenylmethane]bf4.xc6h5no2. *Journal of the American Chemical Society*, *112*(4), 1546–1554. https://doi.org/10.1021/ja00160a038
4. Ion, A. E., Nica, S., Madalan, A. M., Shova, S., Vallejo, J., Julve, M., Lloret, F., & Andruh, M. (2014). Two-dimensional coordination polymers constructed using, simultaneously, linear and angular spacers and cobalt(ii) nodes. new examples of networks of single-ion magnets. *Inorganic Chemistry*, *54*(1), 16–18. https://doi.org/10.1021/ic5025197
5. Kim, H.; Yang, S.; Rao, S. R.; Narayanan, S.; Kapustin, E. A.; Furukawa, H.; Umans, A. S.; Yaghi, O. M.; Wang, E. N. Water Harvesting from Air with Metal-Organic Frameworks Powered by Natural Sunlight. *Science* **2017**, *356*, 430– 434, DOI: 10.1126/science.aam8743
6. Moulton, B., & Zaworotko, M. J. (2001). From molecules to Crystal Engineering: supramolecular isomerism and polymorphism in network solids. *Chemical Reviews*, 101(6), 1629–1658. https://doi.org/10.1021/cr9900432
7. Winarta, J., Shan, B., Mcintyre, S. M., Ye, L., Wang, C., Liu, J., & Mu, B. (2019). A decade of UIO-66 research: A historic review of dynamic structure, synthesis mechanisms, and characterization techniques of an archetypal metal–organic framework. *Crystal Growth & Design*, *20*(2), 1347–1362. https://doi.org/10.1021/acs.cgd.9b00955
8. Gil-San-Millan, R., López-Maya, E., Hall, M., Padial, N. M., Peterson, G. W., DeCoste, J. B., . . . Navarro, J. A. (2017). Chemical warfare agents detoxification properties of zirconium metal–organic frameworks by synergistic incorporation of nucleophilic and basic sites. *ACS Applied Materials & Interfaces*, 9(28), 23967-23973. doi:10.1021/acsami.7b06341
9. Costanzi, S., Machado, J.-H., & Mitchell, M. (2018). Nerve agents: What they are, how they work, how to counter them. *ACS Chemical Neuroscience*, *9*(5), 873–885. https://doi.org/10.1021/acschemneuro.8b00148
10. Chen, Z., Ma, K., Mahle, J. J., Wang, H., Syed, Z. H., Atilgan, A., Chen, Y., Xin, J. H., Islamoglu, T., Peterson, G. W., & Farha, O. K. (2019). Integration of metal–organic frameworks on protective layers for destruction of nerve agents under relevant conditions. *Journal of the American Chemical Society*, 141(51), 20016–20021. https://doi.org/10.1021/jacs.9b11172
11. de Koning, M. C., Peterson, G. W., van Grol, M., Iordanov, I., & McEntee, M. (2019). Degradation and detection of the nerve agent VX by a chromophore-functionalized zirconium MOF. *Chemistry of Materials*, 31(18), 7417–7424. https://doi.org/10.1021/acs.chemmater.9b02073

12. Turner, B. L., Newman, S., & Newman, J. M. (2005). Organic phosphorus sequestration in subtropical treatment wetlands. *Environmental Science & Technology*, *40*(3), 727–733. https://doi.org/10.1021/es0516256
13. Ontario Ministry of Agriculture. (2017, May 5). *Ontario Pesticide Survey (2013/2014)*. Farm & Food Care - Ontario. Retrieved April 30, 2022, from https://www.farmfoodcareon.org/farming-and-the-environment/soil-health/pesticides-in-ontario/
14. Cornwall, W. (2018). Common weed killer—believed harmless to animals—may be harming bees worldwide. Science. https://doi.org/10.1126/science.aav5169
15. Troya, D. (2016). Reaction mechanism of nerve-agent decomposition with ZR-based Metal Organic Frameworks. *The Journal of Physical Chemistry C*, 120(51), 29312–29323. https://doi.org/10.1021/acs.jpcc.6b10530
16. Li, L., Tang, S., Wang, C., Lv, X., Jiang, M., Wu, H., & Zhao, X. (2014). High gas storage capacities and stepwise adsorption in a uio type metal–organic framework incorporating Lewis Basic Bipyridyl sites. *Chemical Communications*, 50(18), 2304. https://doi.org/10.1039/c3cc48275h
17. Shearer, G. C., Chavan, S., Ethiraj, J., Vitillo, J. G., Svelle, S., Olsbye, U., Lamberti, C., Bordiga, S., & Lillerud, K. P. (2014). Tuned to perfection: Ironing out the defects in metal–organic framework UIO-66. *Chemistry of Materials*, 26(14), 4068–4071. https://doi.org/10.1021/cm501859p
18. Kalaj, M., Palomba, J. M., Bentz, K. C., & Cohen, S. M. (2019). Multiple functional groups in uio-66 improve chemical warfare agent simulant degradation. *Chemical Communications*, 55(37), 5367–5370. https://doi.org/10.1039/c9cc02252j
19. Learn XPS. Thermo Scientific XPS: What is XPS. (n.d.). https://xpssimplified.com/whatisxps.php.
20. Meng, Y., Wang, M., Tang, M., Hong, G., Gao, J., & Chen, Y. (2017). Preparation of robust superhydrophobic halloysite clay nanotubes via mussel-inspired surface modification. *Applied Sciences*, 7(11), 1129. https://doi.org/10.3390/app7111129
21. Wang, Y., Li, L., Dai, P., Yan, L., Cao, L., Gu, X., & Zhao, X. (2017). Missing-node directed synthesis of hierarchical pores on a zirconium metal–organic framework with tunable porosity and enhanced surface acidity via a microdroplet flow reaction. *J. Mater. Chem. A*, 5(42), 22372–22379. https://doi.org/10.1039/c7ta06060b
22. Luan, Y., Qi, Y., Gao, H., Andriamitantsoa, R. S., Zheng, N., & Wang, G. (2015). A general post-synthetic modification approach of amino-tagged metal–organic frameworks to access efficient catalysts for the KNOEVENAGEL condensation reaction. *Journal of Materials Chemistry A*, 3(33), 17320–17331. https://doi.org/10.1039/c5ta00816f
23. CEM. (2021). *Discover 2.0 Microwave Synthesizer Manual*. CEM Corporation.
24. Li, Y., Liu, Y., Gao, W., Zhang, L., Liu, W., Lu, J., Wang, Z., & Deng, Y.-J. (2014). Microwave-assisted synthesis of UIO-66 and its adsorption performance towards dyes. *CrystEngComm*, *16*(30), 7037–7042. https://doi.org/10.1039/c4ce00526k
25. Koppe, J., Bußkamp, M., & Hansen, M. R. (2021). Frequency-swept ultra-wideline magic-angle spinning NMR spectroscopy. *The Journal of Physical Chemistry A*, *125*(25), 5643–5649. https://doi.org/10.1021/acs.jpca.1c02958
26. Barone, G., Mastalerz, R., Reiher, M., & Lindh, R. (2008). Nuclear quadrupole moment of 119Sn. *The Journal of Physical Chemistry A*, *112*(7), 1666–1672. https://doi.org/10.1021/jp710388t

27. Stassen, I., Bueken, B., Reinsch, H., Oudenhoven, J. F., Wouters, D., Hajek, J., Van Speybroeck, V., Stock, N., Vereecken, P. M., Van Schaijk, R., De Vos, D., & Ameloot, R. (2016). Towards metal–organic framework based field effect chemical sensors: UIO-66-NH2 for nerve agent detection. *Chemical Science*, *7*(9), 5827–5832. https://doi.org/10.1039/c6sc00987e
28. Harshit, D., Charmy, K., & Nrupesh, P. (2017). Organophosphorus pesticides determination by novel HPLC and spectrophotometric method. *Food Chemistry*, *230*, 448–453. https://doi.org/10.1016/j.foodchem.2017.03.083
29. Mercuri, G., Moroni, M., Galli, S., Piccirillo, C., Capodilupo, A.-L., Tuci, G., Giambastiani, G., & Rossin, A. (2022). Uio-67-derived bithiophene and bithiazole mixmofs for Luminescence Sensing and removal of contaminants of emerging concern in wastewater. *Inorganic Chemistry Frontiers*, *9*(1), 90–102. https://doi.org/10.1039/d1qi01184g
30. Tan, B., Luo, Y., Liang, X., Wang, S., Gao, X., Zhang, Z., & Fang, Y. (2020). One-pot synthesis of two-linker mixed al-based metal–organic frameworks for modulated water vapor adsorption. *Crystal Growth & Design*, *20*(10), 6565–6572. https://doi.org/10.1021/acs.cgd.0c00747
31. Sun, D.-W., Huang, L., Pu, H., & Ma, J. (2021). Introducing reticular chemistry into agrochemistry. *Chemical Society Reviews*, *50*(2), 1070–1110. https://doi.org/10.1039/c9cs00829b